Quantitative characterization of the 3D self-organization of PDAC tumor spheroids reveals cell type and matrix dependence through advanced microscopy analysis

Cite as: APL Bioeng. **9**, 016116 (2025); doi: 10.1063/5.0242490
Submitted: 4 October 2024 · Accepted: 28 February 2025 ·
Published Online: 27 March 2025

Soraya Hernández-Hatibi,[1,2] Carlos Borau,[1,3] Neus Martínez-Bosch,[4] Pilar Navarro,[4,5,6] José Manuel García-Aznar,[1,7,a)] and Pedro Enrique Guerrero[1,2,7]

AFFILIATIONS

[1]Multiscale in Mechanical & Biological Engineering Research Group, Aragon Institute of Engineering Research (I3A), School of Engineering and Architecture, University of Zaragoza, Zaragoza, Aragon, Spain
[2]Department of Biochemistry and Molecular and Cellular Biology, University of Zaragoza, Zaragoza, Spain
[3]Centro Universitario de la Defensa de Zaragoza, 50090 Zaragoza, Spain
[4]Cancer Research Program, Hospital del Mar Research Institute (HMRI), Unidad Asociada IIBB-CSIC, 08003 Barcelona, Spain
[5]Department of Molecular and Cellular Biomedicine, Institut of Biomedical Research of Barcelona (IIBB-CSIC), 08036 Barcelona, Spain
[6]Institut d'Investigacions Biomèdiques August Pi Sunyer (IDIBAPS), 08036 Barcelona, Spain
[7]Aragon Institute for Health Research (IIS Aragon), Miguel Servet University Hospital, Zaragoza, Aragon, Spain

[a)]**Author to whom correspondence should be addressed:** jmgaraz@unizar.es

ABSTRACT

Pancreatic ductal adenocarcinoma (PDAC) is characterized by an abundant tumor-associated stroma composed from pancreatic stellate cells, which play a critical role in tumor progression. Developing accurate *in vitro* models requires understanding the complex interactions between tumor cells and their microenvironment. In this study, we present a quantitative imaging-based characterization of the three dimensional (3D) self-organization of PDAC tumour spheroids using a microfluidic platform that mimics key aspects of the tumor microenvironment. Our model incorporates collagen type I hydrogels to recreate the extracellular matrix, activated human pancreatic stellate cells (HPSCs), and various tumor cell types. Advanced imaging techniques, including Lattice Lightsheet Microscopy, allowed us to analyze the 3D growth and spatial organization of the spheroids, revealing intricate biomechanical interactions. Our results indicate that alterations in matrix properties—such as stiffness, pore size, and hydraulic permeability—due to variations in collagen concentration significantly influence the growth patterns and organization of PDAC spheroids, depending on tumor subtype and epithelial–mesenchymal phenotype. Higher collagen concentrations promoted larger spheroids in epithelial-like cell lines, while mesenchymal-type cells required increased collagen for self-organization into smaller spheroids. Furthermore, coculture with HPSCs affected spheroid formation distinctly based on each PDAC cell line's genetic and phenotypic traits. HPSCs had opposing effects on epithelial-like cell lines: one cell line exhibited enhanced spheroid growth, while another showed inhibited formation, whereas mesenchymal-like spheroids showed minimal impact. These results provide insights into tumor–stroma interactions, emphasizing the importance of the cell-specific and matrix-dependent factors for advancing our understanding of PDAC progression and informing future therapeutic strategies.

INTRODUCTION

Pancreatic cancer is a highly aggressive and devastating cancer. Currently, it ranks as the third-leading cause of cancer-related death. However, without substantial advancements in diagnostic and therapeutic methods, it is expected to ascend to the second position in the near future.[1] The most prevalent type of pancreatic cancer (> 90%) is

pancreatic ductal adenocarcinoma (PDAC), an aggressive invasive neoplasm characterized by a poor prognosis and a 5-year relative survival rate of only 12%.[2]

One of the main reasons for the high resistance of PDAC to both chemotherapy and immunotherapy is its complex tumor microenvironment.[3] PDAC microenvironment is particularly fibrotic, with a desmoplastic stroma that counts for up to 90% of pancreatic tumor volume and supports tumor progression and immune evasion.[4,5] This desmoplastic reaction is characterized by a complex and dynamic interplay of various components, including activated cancer-associated fibroblasts (CAFs), immune cells, and extracellular matrix (ECM) components.[6–8] This intricate process entails the activation and recruitment of different populations of CAFs, such as the pancreatic stellate cells (PSCs), which results in the excessive deposition, remodeling, and degradation of the ECM.[9] Simultaneously, PDAC desmoplasia triggers exaggerated inflammatory responses, abnormal immune reactions, and disruptions in angiogenesis and blood supply, contributing to compromised drug delivery and efficacy.[5,10]

PSCs are one of the most abundant and active components of the PDAC microenvironment. These cells maintain tissue structure, regulate the synthesis and degradation of the ECM, and participate in tissue repair and regeneration in healthy tissue. When they interact with tumor cells, PSCs are activated by several factors such as cytokines, chemokines, growth factors, and other molecules secreted by cancer cells, immune cells, and endothelial cells. Activated PSCs undergo a significant transformation resembling an activated myofibroblast-like phenotype. This transformation is marked by noteworthy alterations in morphology, resulting in a spindle shape, elevated cell motility, and proliferation rates.[11] Activated PSCs play a crucial role in the excessive synthesis of ECM components, such as the various types of collagens, proteoglycans, glycoproteins, and hyaluronic acid.[12,13] The dysregulated stiffness, composition, and organization of the ECM can generate a tumor-friendly microenvironment, which has been implicated in PDAC initiation, progression, invasion, and metastasis.[14–16] Therefore, in recent years, pancreatic cancer research has focused on the dynamic interplay between tumor cells and stromal components in the development, progression, and metastatic capacity of PDAC. Despite significant advancements in the understanding of the dynamics and heterogeneity of the PDAC microenvironment, there remain many unknown aspects of the relationship between the stroma components (cellular, chemical, mechanical, and architectural properties) and tumor development in PDAC.[17,18] Further insights into this complex interaction would help to better understand key aspects of this disease, thus aiding in the development of new therapeutic and diagnostic strategies.[19,20]

In order to improve our understanding of the stromal-tumor interaction and assess the key factors in this interplay that promote the development and malignancy of PDAC, it is necessary to use *in vitro* models that allow us to recapitulate biological processes during tumor development. In recent years, there has been a breakthrough in the development of three-dimensional (3D) *in vitro* cultures that have overcome some of the limitations of traditional two-dimensional (2D) cultures.[21–23] This approach offers a more physiological alternative, replicating the development of solid tumors, an inherently three-dimensional process. One such innovative 3D culture strategy is based on microfluidics. This technique allows for precise control over various chemical, mechanical, and cellular variables, thereby more accurately mimicking the *in vitro* tumor environment.[24–26]

In this study, we aim to develop a humanized microfluidic approach that closely mimics the intricate particularities of the PDAC microenvironment, featuring a defined 3D architecture that is spatially organized. For this aim, we have generated a simplified microfluidic-based 3D model that integrates some key components of PDAC microenvironment, such as collagen type I (Col I) hydrogels, to mimic the ECM, activated human pancreatic stellate cells (HPSCs), and pancreatic tumor cells. For our model, we selected four human PDAC cell lines (BxPC-3, Capan-2, Panc-1, and MIA PaCa-2) with different genetic complexity and different tumor subtypes (classical and squamous) regarding their histopathological differentiation grade and expression of epithelial–mesenchymal transition (EMT) related markers, i.e., the difference lies in the loss of polarity and adhesion between cells and in the gain of migratory and invasive capacities.[27] Specifically, we analyzed the role of the interaction between the mechanical characteristics given by the collagen concentration of the ECM and the HPSCs population in triggering different cellular responses related to the growth of the tumor cells in a 3D environment. These collagen-based hydrogels matrices present differences on their mechanical and microstructural properties.[28,29] By altering the collagen concentration, we noticed differences in spheroid growth and organization related to variations in mechanical and architectural properties resulting from changes in the concentration of Col I within the matrix. Moreover, the influence of HPSCs on direct coculture had divergent outcomes based on the PDAC cell line under study concerning tumor spheroid formation and growth. Our results demonstrate the intricate, cell line-specific interactions between PDAC cells, HPSCs, and the properties of the collagen matrix, highlighting the critical role of these elements in the tumor microenvironment. Therefore, this model can help deepen our understanding of the biomechanical stromal factors that regulate PDAC growth and progression.

METHODS

Microfluidic device fabrication

The geometry of the microfluidic devices was based on that used by Farahat *et al.*,[30] which consists of a central chamber (2.5 × 1.3 mm) containing the hydrogel and two side media channels running parallel to the central chamber. The height of the channels is 300 μm all over the geometry.

Microdevices were fabricated following the methodology described by Shin *et al.*[24] Briefly, microfluidic devices were prepared using polydimethylsiloxane (PDMS, Dow Corning) at a 10:1 weight ratio for the base to curing agent. The mixed solution was degassed to remove air bubbles, poured in a SU-8 master, where the desired microengineered geometry was patterned with a soft photolithography technique and cured overnight at 80 °C. Once the solution was cured, the molded replica was perforated using disposable biopsy punches to create the inlet and outlet ports. PDMS microdevices were autoclaved, and finally bonded to a 35 mm glass-bottom Petri dish (Ibidi) by plasma treatment (PDC-32G Basic Plasma Cleaner, Harrick Plasma, NY, USA). The formed microgeometry was then coated with 0.5 mg/ml poly-dopamine solution in 10 mM Tris-HCl pH 8.5 (PDA, Sigma-Aldrich, Spain) to enhance collagen adhesion onto the channel surface as described in Ref. 31. The microfluidic devices were then ready to be used after washing and drying overnight in an oven at 60 °C to restore the hydrophobicity of the bonded surfaces.

Three-dimensional culture in the microfluidic devices

Cell culture

The human pancreatic cancer cell lines BxPC-3, Capan-2, Panc-1, and MIA PaCa-2 were purchased from the American Type Culture Collection. Capan-2 and BxPC-3 are commonly associated with a more epithelial phenotype, with Capan-2 typically characterized as a well-differentiated tumor (Grade 1, G1) and BxPC-3 as a moderately differentiated tumor (Grade 2, G2). Panc-1 and MIA PaCa-2 are considered poorly differentiated tumor cell lines (Grade 2, G2-Grade 3, G3), both of which are associated with a mesenchymal EMT status.[27,32,33] The activated HPSCs was a kind gift of Dr. R. F. Hwang (University of Texas MD Anderson Cancer Center, Houston, Texas, USA).[34]

All the cell lines were cultured using high-glucose Dulbecco's Modified Eagle Medium (DMEM, Gibco, Spain) (4.5 g/l D-Glucose, L-Glutamine, Pyruvate) supplemented with 10% fetal bovine serum (FBS, Life technologies, Spain). Cell culture was maintained in a humidified atmosphere incubator at 37 °C and with 5% CO_2.

Hydrogel preparation and cell seeding

The hydrogels used were prepared using a stock of rat tail collagen type I (Corning, Spain) at a final collagen concentration of 2.5, 4, and 6 mg/ml with high-glucose DMEM medium, 10× Dulbecco's phosphate buffered saline (DPBS, Sigma-Aldrich, Spain) (1/10 of the final volume), and NaOH 0.5M (Sigma-Aldrich, Spain), at pH 7.4.[24] Individual pancreatic cancer cells (approximately 750 cells/device) were mixed with the collagen hydrogel solution following the strategy presented by Plou *et al.*[35] For coculture with HPSCs, a 2:1 ratio of HPSCs to tumor cells was used. The mixing of the hydrogel with the cells was then pipetted into the central chamber through the loading ports (Fig. 1), and the devices were placed in humidity chambers in an incubator at 37 °C and 5% CO_2 for 20 min to allow the collagen polymerization. To prevent cell sedimentation during polymerization and ensure homogeneous distribution within the hydrogel, the microfluidic devices were rotated every few minutes during this process. This method prevents gravitational settling, keeping the cells uniformly distributed and embedded within the central region of the chamber. After that, the hydrogels were hydrated with culture medium (high-glucose DMEM, Gibco) and stored in the incubator for 10 days. The cultured medium was renewed every 48 h through the reservoirs (Fig. 1).

Microscopy and image analysis

Growth analysis of the 3D tumoral spheroids

The growth and morphology of the PDAC cell lines were monitored over 10 days by acquiring brightfield images at 4× magnification every 48 h with an optical inverted microscope (DM IL LED, Leica, Wetzlar, Germany) to characterize the formation of 3D tumor spheroids within the collagen hydrogels. Tumor cell cluster and spheroid sizes were analyzed using a custom semi-automated script designed for segmentation in MATLAB based on active contour techniques. Additionally, the average diameters of all the cell lines were measured at seeding using the automated cell counting software of the Countess 3 cell counter (Thermo Fisher Scientific). These measurements were used to calculate the cell radius, which was rounded to the nearest whole number, to determine the mean surface area for each cell line, as detailed in Table S.1. Segmented components that exceeded the designated area of an isolated cell were considered potential cellular clusters capable of transforming into spheroids over time within the microfluidic device during the culture period. It is important to note that new spheroids may appear at any time, and we did not individually track them. This implies that spheroids at different stages of their evolution and therefore varying sizes are present by the end of the experiments.

Eccentricity was used as a measure to quantify the shape of cellular spheroids. It is calculated as the ratio of the distance between the foci of the ellipse that has the same second moments as the region, and its major axis length. The value of eccentricity ranges between 0 and 1, with 0 representing a perfect circle and 1 indicating a line segment.

3D topographic analysis of spheroid organization

We employed a custom-made MATLAB script to perform the 3D topographic analysis of spheroid organization. The primary segmentation of nuclei was achieved using basic thresholding techniques. Then, to split overlapping objects, we utilized the segmented volume and identified the nuclei centers by applying multiscale Laplacian of Gaussian methods. Subsequently, a 3D watershed algorithm was applied using these nuclei centers as markers.

For the analysis of spheroid topology and neighbor relationships, we employed an increasing search radius in three dimensions, starting from the nuclei centers, until all nuclei were connected into a single component [see Figs. 9(d) and S.3]. This radius value, referred to as R1CC, provided an approximation of the compactness of the spheroid structure, offering insights into the spatial organization and cohesiveness of the spheroids. Thus, lower R1CC values indicated greater compactness. Additionally, to analyze the total volume occupied by the overall spheroid, the alpha shape (a generalization of the convex hull that allows for the creation of a tight-fitting boundary around a set of points) was computed.

Fluorescence staining and Lattice lightsheet fluorescence microscopy

Structural analysis of PDAC spheroids studied under the different conditions was carried out using different fluorescent stains. Imaging of the staining samples were taken using a Lattice Lightsheet 7 microscope equipped with a 40× objective (Zeiss, Germany).

3D culture samples were fixed in 4% paraformaldehyde (PFA, Sigma-Aldrich, Spain) for 20 min at room temperature, washed with 1× phosphate buffered saline solution (PBS, Gibco, Spain) and permeabilized with 0.1% Triton X-100 (Calbiochem, Spain) for 10 min at room temperature (RT) in agitation. The samples were washed and then blocked in 5% bovine serum albumin fraction V (BSA, Merck, Spain), 0.01% Triton X-100 in PBS, (Gibco, Spain) overnight (o/n) at 4 °C. Afterwards, they were incubated with rhodamine phalloidin (0.125 mg/ml, ChemCruz USA, dilution 1:100) to stain F-actin cytoskeleton and DRAQ5™ 20 μM for nuclei staining (5 mM, ThermoFisher Scientific, Spain). Finally, the samples were washed three times with PBS and stored at 4 °C until image acquisition.

Immunofluorescence staining for HPSCs and tumor cell colocalization analysis

To assess the spatial distribution of HPSCs in relation to tumor spheroids, additional immunofluorescence staining was performed for α-SMA (a marker of activated PSCs) and CK19 (a marker of PDAC epithelial cells). After fixation, permeabilization, and blocking, samples were

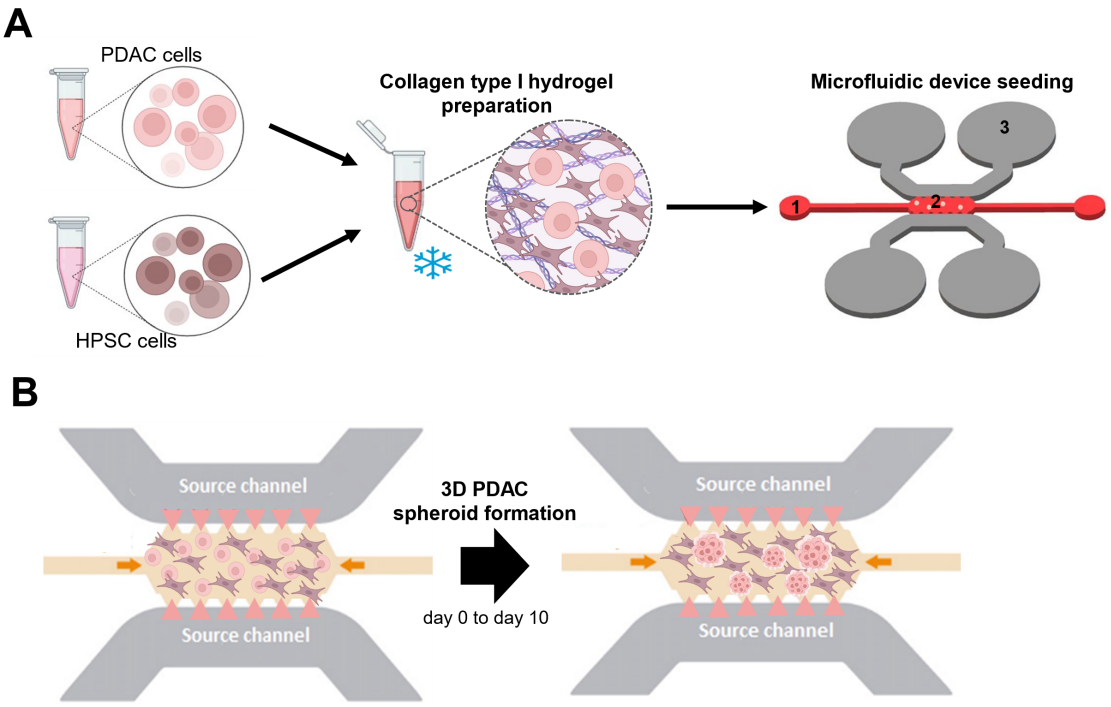

FIG. 1. Tumor-on-a-chip experimental setup. (a) Hydrogel preparation and cell seeding inside the microfluidic device. Tumor PDAC cells and HPSCs were collected and mixed with the Col I hydrogel solution. For monoculture, only PDAC cells were introduced. The hydrogel mixture with the cells was introduced through the loading port (1) of the microfluidic device into the central chamber (2), where it polymerized. The cells were embedded three dimensionally in the hydrogel. Once the hydrogel had polymerized, medium was added through the reservoirs (3) to hydrate the hydrogel and maintain the cell culture. (b) The PDAC cells, in monoculture or direct HPSCs coculture, formed self-organized three-dimensional spheroids within the biomimetic Col I hydrogel from isolated cells.

incubated o/n at 4 °C with primary antibody against CK19 (dilution 1:100, Abcam ab76539) in blocking buffer (1% BSA, 0.01% Triton X-100 in PBS). The next day, samples were washed with PBS and incubated with Alexa Fluor 647-conjugated secondary antibody (dilution 1:200, Life Technologies A31573) and α-SMA-Cy3 (dilution 1:100, Sigma C6198, Spain) in blocking buffer for 2 h at RT in the dark. Samples were washed with PBS and stored at 4 °C until imaging.

Images were acquired using a confocal microscope STELLARIS 5 DLS (Leica Microsystems CMS, Germany) equipped with a 10× objective. Some images were further magnified using a 2× digital zoom to enhance visualization of specific cellular structures.

Image processing and colocalization analysis

To differentiate between HPSCs and tumor-derived α-SMA expression, a colocalization analysis was performed. CK19 fluorescence was used to generate a binary mask identifying tumor spheroids structures. This mask was then subtracted from the α-SMA signal to isolate α-SMA expression in non-spheroids regions. The colocalization analysis and image processing were carried out using Fiji software, allowing for the precise localization of HPSCs within our microfluidic system.

Data and statistical analysis

Biological replicates of all conditions presented in this paper have been carried out in duplicate with three technical replicates every time. Data and statistical analyses, including the segmentation analysis of spheroid area and eccentricity, were performed using the statistical software GraphPad Prism v8.0.1 in combination with Microsoft Excel software. First, the normality of the data was assessed with the Shapiro–Wilk or Kolmogorov tests, depending on the amount of data. Also, Levenés test was performed to analyze the homogeneity of the variance. After normality and homogeneity of the variance test, analysis of variance (ANOVA) was performed to determine statistical significance among the studied continuous variables in the different conditions. Depending on the information raised from the normality and homogeneity of variance analyses, different parameters for the ANOVA test were applied: Welch ANOVA with Games-Howell as post hoc tests, ordinary ANOVA followed by post hoc Tukey–Kramer tests, Kruskal–Wallis tests with post hoc Dunn's test. In some cases, a t-test was used followed by a Mann–Whitney U test. A p value (α) below 0.05 was considered a significant result. Results presented in violin plots show median (continuous line), quartiles Q1 and Q3 (dash lines), and the maximum and minimum values.

RESULTS

Collagen concentration regulates PDAC spheroid morphology and growth by tumor cell type

To examine the impact of varying concentrations of collagen on the 3D growth pattern of PDAC, an analysis on the 3D self-organization capability of tumor spheroids using different human

PDAC (hPDAC) cell lines was conducted. The objective was to enhance comprehension regarding the influence of ECM structural and mechanical factors on tumor growth by assessing the capacity of different PDAC cell lines (BxPC-3, Capan-2, Panc-1, and MIA PaCa-2) to develop spheroids. To test this, we embedded the cell lines into hydrogels containing different concentrations of Col I (2.5, 4, and 6 mg/ml) in our microfluidic devices. Using this approach, tumor cells organized into 3D tumor spheroids from single cells, due to proliferation driven by biomechanical cues from their environment.

By modifying the collagen concentration of the matrix, different fates were observed in cell aggregation and spheroid formation in all the tested cell lines (Fig. 2). Cells distribution within the hydrogel was analyzed 24 h after seeding to confirm that these effects were not due to differences in initial cell distribution caused by sedimentation. Our analysis of the first 50 μm of the central chamber revealed that the number of cells in the region closest to the glass surface (0–20 μm) was very low across all cell lines and conditions [Figs. S5(c) and S5(e)]. This confirmed that our chamber rotation method during hydrogel polymerization effectively prevents sedimentation, ensuring that cells remain embedded within the hydrogel rather than accumulating at the bottom. Additionally, cells were predominantly located at depths further from the glass ($Z \geq 10$ μm) [Figs. S5(c) and S5(e)]. This confirmed that they were distributed within the hydrogel rather than in the regions where 2D growth typically occurs. To further confirm that initial cell numbers were comparable across conditions, we also performed an Alamar Blue assay 24 hours after the seeding. The fluorescence intensity values showed no significant differences between conditions, indicating that all groups started with a similar number of cells [Fig. S5(b) and S5(d)].

We observed that only cell lines exhibiting a moderate and well differentiated histomorphology grade related to an epithelial phenotype, BxPC-3 and Capan-2, were able to form spheroids in all the matrices tested after 10 days of culture [Fig. 2(a), top panel]. As the grade of differentiation is lost and the cell lines express mesenchymal markers, such as Panc-1 and MIA Paca-2 cells, higher concentrations of collagen were required to observe the ability for 3D self-assembly, resulting in spheroid formation [Fig. 2(a), bottom panel]. Significantly, the Panc-1 cell line, which is recognized in the literature as being in an intermediary stage between the epithelial and mesenchymal phenotypes, can produce certain spheroid-like structures in lowest collagen matrices. However, increased collagen is necessary for proper spheroid formation.

Investigating how ECM mechanical factors, such us collagen type I concentration, affect PDAC growth, we analyzed spheroid growth by measuring its area over a 10-day culture period. Given that our study involved a population analysis rather than individual spheroid tracking, relying solely on the median could introduce bias, particularly in cases where many new and smaller spheroids were generated over time. To provide a more accurate representation of the PDAC cell lines' ability to form larger spheroids under each culture condition, we also analyzed the 90th percentile (p90) values. Notably, the examination of collagen concentrations' effect revealed diverse growth responses among all tested PDAC cell lines, each exhibiting distinct growth patterns [Fig. 2(b)]. The growth of BxPC-3 spheroids was more uniform in matrices with lower collagen concentration (2.5 mg/ml), although these matrices had reduced spheroid formation, as evidenced by lower median and p90 values [Fig. 2(b), BxPC-3]. As collagen concentration increased, this cell line exhibited a tendency to form spheroids with more pronounced growth [Fig. 2(b), BxPC-3] and increased size variability [Fig. S1(a)], especially in the first days of culture in the higher collagen matrix (6 mg/ml). The increased p90 values in higher collagen matrices (4 and 6 mg/ml) suggested a heightened potential for larger spheroid formation [Fig. 2(b), BxPC-3]. For the Capan-2 cell line, increased collagen concentration correlated with a more homogeneous population [Fig. S1(a)]. However, the growth trend over time was similar across matrices [Fig. 2(b), Capan-2], indicating comparable spheroid growth regardless of collagen concentration. The consistently high p90 values, particularly in the 6 mg/ml matrix, suggest a high potential for larger spheroid formation [Fig. 2(b), Capan-2].

The Panc-1 cell line showed high spheroid growth rates in both collagen matrices (4 and 6 mg/ml), with increasing median and p90 values over time. The 6 mg/ml matrix had slightly slower but more uniform growth [Fig. S1(a)], while the 4 mg/ml matrix had greater potential for larger spheroids at culture endpoints [Fig. 2(b), Panc-1]. Finally, the MIA PaCa-2 cells exhibited results similar to Panc-1. At early culture times, the 6 mg/ml matrix led to faster growth and slightly larger spheroids, but over time, the median and p90 values decreased compared to the 4 mg/ml matrix, where growth remained more consistent, and the potential for larger spheroids increased [Fig. 2(b), MIA PaCa-2]. This cell line also showed an increase in size variability with higher collagen concentration, similar to BxPC-3 spheroids [Fig. S1(a)]. It is noteworthy that the Panc-1 and MIA PaCa-2 cell lines were not suitable for examination in the 2.5 mg/ml matrices, as these cell types lacked the ability to self-organize in 3D within lower collagen matrices [Fig. 2(a), bottom panel]. Particularly, in the Panc-1 cell line, spheroid-like structures were observed at the end point; however, quantification over time was not feasible due to 2D cell proliferation.

To further investigate the growth patterns of different human PDAC cell lines in varying collagen concentrations, we analyzed the size and morphology of the spheroids formed at day 10 (Fig. 3). Morphological analysis was conducted using the concept of eccentricity, which indicates whether the spheroids are more spherical or elliptical in shape. The BxPC-3 cells were able to form spheroids in all the matrices used. There was a dual population of spheroids of different sizes, which polarized toward the larger spheroids as the collagen concentration increased [Fig. 3(a), BxPC-3]. As the concentration of collagen in the matrices increased, the spheroids generated by this cell line grew in size significantly [Fig. 3(b), BxPC-3), and they showed a more irregular morphology [Fig. 3(c), BxPC-3]. For the other epithelial phenotype cell line, Capan-2, observations suggested that spheroids in the 4 mg/ml collagen concentration matrix were slightly smaller [Fig. 3(a), Capan-2]. Although quantification of spheroid areas and eccentricity in each matrix condition revealed no significant differences [Figs. 3(b) and 3(c), Capan-2].

For the quasi-mesenchymal phenotype cell line Panc-1, it was found that the mechanical properties of the 2.5 mg/ml collagen matrix were insufficient to facilitate proper 3D self-organization [Fig. 3(a), Panc-1]. In this low-collagen matrices, spheroids formed were more similar to cell aggregates, and over time, most cells tended to migrate to a 2D layer at the bottom of the glass device [Fig. 3(a), Panc-1]. In other words, higher collagen concentrations were required for the formation of proper tumor spheroids. In this particular cell line, a slight difference in size distribution was observed in the spheroids when

comparing matrices with collagen concentrations of 4 and 6 mg/ml [Fig. 3(b), Panc-1], although no significant differences in morphology were observed [Fig. 3(c), Panc-1]. The mesenchymal cell line MIA PaCa-2 [Fig. 3(a)] also needed increased collagen concentration to produce spheroids. In this case, the same Panc-1 trend was observed, the spheroids formed in the 4 mg/ml matrix were larger compared with the 6 mg/ml [Fig. 3(b), MIA PaCa-2]. This condition also produced statistically fewer round spheroids compared to 6 mg/ml [Fig. 3(c), MIA PaCa-2].

To achieve further insights into the understanding of how spheroids self-organize according to the biophysical properties of the matrix, we carried out a preliminary study of its structural topography. The study involved 3D spheroid reconstructions based on Lattice light-sheet microscopy [Fig. 4(a)] that allowed us to make a first analysis of the connectivity of the nuclei forming the spheroids obtained at different collagen matrices by nuclear segmentation techniques [Fig. 9(a)]. The overall size and shape of the BxPC-3 spheroid segmentation [Fig. 9(a)] agrees with the size quantification in these conditions (Fig. 3). The individual segmentation of nuclei, however, suggests that bigger spheroids, produced within the 6 mg/ml collagen matrices, are composed of many (>100), highly compacted cells [Fig. 4(b)]. In fact, we observed a rapid decrease in the number of connected components as the search radius increases, with 14.7 μm being the radius at which all the nuclei are connected (R1CC) [Fig. 4(b), BxPC-3]. In other

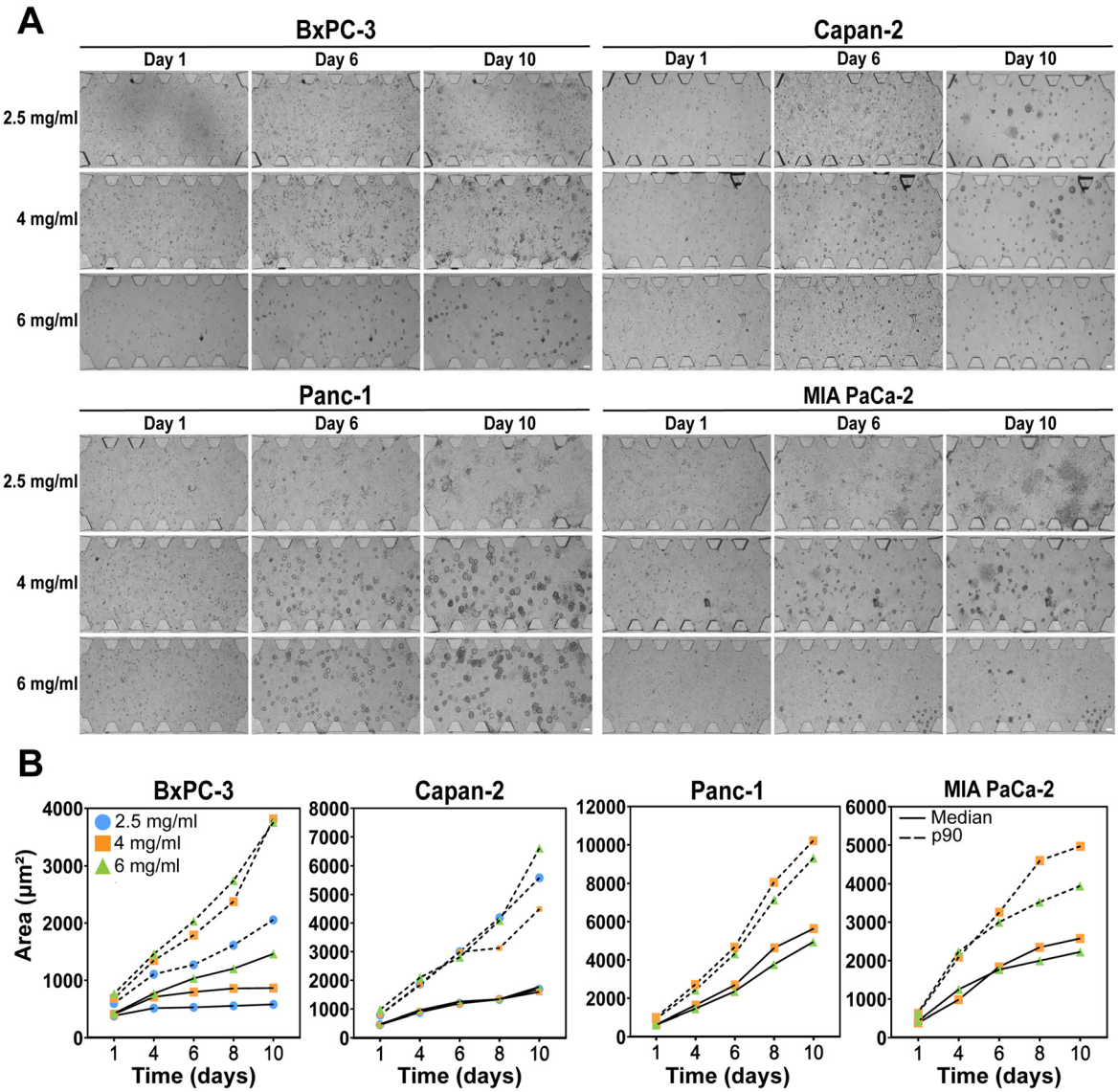

FIG. 2. 3D culture of PDAC tumor spheroids in collagen-based microfluidic devices over time. (a) Brightfield images of different tumor PDAC cell line spheroid growth over time (up to 10 days) in 2.5, 4, and 6 mg/ml collagen matrices (scale bar 200 μm). (b) Evolution over time of the PDAC spheroids area in the different collagen-based matrices. Continuous lines show the median values, and dashed lines represent the 90% percentile (p90) of the different cell lines in each culture condition.

words, the average distance between cell nucleus was lower than 14.7 μm in this condition, with R1CC values of 16.24 μm and 19.6 μm for the 4 and 2.5 mg/ml conditions, respectively. The average number of cell nuclei neighbors at this distance is ≈4 for the denser matrices, and ≈2 for the 2.5 mg/ml case, as the number of nuclei is significantly lower [Figs. 9(a) and 9(c)]. The Capan-2 cell line, which produced similar spheroid sizes across the different collagen matrices [Fig. 3(b), Capan-2], showed, however, some differences regarding nuclei organization, with the largest amount (>70) and more aggregated nuclei (R1CC = 15.4 μm) corresponding to the 4 mg/ml case, as opposed to a less dense structure in the case of 6 mg/ml (note the slower fall of the curve until R1CC = 20.86 μm) [Fig. 4(b), Capan-2]. The number of neighbors at R1CC varied mostly between 3 and 5 for the different collagen concentrations [Fig. 9(c)].

Data obtained for the more mesenchymal cell lines, Panc-1 and MIA PaCa-2, shows similar trends. A quantity of 6 mg/ml collagen matrices produce more compacted spheroids (smaller R1CC values) compared to 4 mg/ml cases [Fig. 4(b), Panc-1 and MIA PaCa-2]. Specifically, Panc-1 resulted in R1CC = 20.86 μm and 22.4 μm for 6 and 4 mg/ml, respectively, while MIA PaCa-2 resulted in R1CC = 16.24 μm and 22.4 μm for 6 and 4 mg/ml. It is worth noting that all these spheroids contain about 50 cells each [Fig. 4(b)], except for the MIA PaCa-2 at 6 mg/ml, which contains only 29 [Fig. 4(b)].

Overall, our observations suggest that in our tumor model, the effects of the ECM mechanical characteristics on cell growth and proliferation vary according to the tumor cell subtype and the collagen composition of the matrix. Under identical conditions, some cell lines exhibited enhanced growth and proliferation, while others did not.

Pancreatic stellate cells promote differential effects on spheroid growth dynamics depending on PDAC tumor subtype

To investigate the interaction between stromal components and tumor cells beyond the intrinsic properties of the ECM, we developed a more complex microfluidic-based 3D model. This advanced model included α-SMA$^+$ positive activated HPSCs[36] in addition to biomimetic matrices, better mimicking the complex PDAC stroma microenvironment. By incorporating these HPSCs into our model, we aimed to simulate the activated state of PSCs and replicate the ECM remodeling dynamics that contribute to the PDAC tumor microenvironment. We selected the 6 mg/ml collagen matrices for this model because PDAC is characterized by a dense and fibrotic ECM, primarily composed of Col I secreted by PSCs.[37] A higher concentration of collagen provides mechanical properties more similar to those found in the PDAC stroma. This approach allows us to better understand the complex interplay between cancer cells and stromal components, providing a more faithful representation of the PDAC stromal niche in our experimental setting.

Considering the abundant stroma present in PDAC, we optimized the incorporation of HPSCs in a ratio to tumor cells of 2:1 in our microfluidic device (data non shown). It was observed that the activated HPSCs were distributed throughout the hydrogel, acquiring a spindle shape, characteristic of their myofibroblast-like phenotype [Fig. 5(a)]. In contrast, PDAC cells continued to self-organize in 3D, forming tumor spheroids [Figs. 6(a) and 7(a)]. To further characterize the distribution of HPSCs within the hydrogel, we performed immunofluorescence staining for α-SMA and CK19, followed by a colocalization analysis. α-SMA is commonly used as a marker for activated PSCs; however, its expression was also detected in tumor spheroids, both in monoculture (data non shown) and in coculture conditions [Fig. 5(a)]. To differentiate stromal α-SMA expression from tumor-derived α-SMA signal, CK19 immunostaining was performed, as this marker is exclusively expressed in PDAC cells [Fig. 5(a)]. Fluorescence images showed that HPSCs were distributed throughout the hydrogel and did not integrate into the tumor spheroids. Instead, they remained within the matrix, surrounding the spheroidal structures of PDAC cells [Fig. 5(b)]. In contrast, CK19-positive tumor cells were exclusively confined within the spheroids, indicating that only PDAC cells formed these 3D structures [Fig. 5(b)].

As done for the previous conditions, we measured spheroids' areas over 10 days, and we observed the effect on the behavior of the different PDAC cell lines with and without HPSCs [Fig. 6(a)]. Representation of growth curves revealed interesting patterns in the behavior of the different cell lines [Figs. 6(b) and S1(b)]. For example, for the epithelial BxPC-3 cells, the presence of the HPSCs reduced the formation of spheroids. In monoculture, at initial stage of the culture period, a cluster population of cells with a median size of approximately 500 μm^2 was observed. As culture time progressed, this population persisted and larger spheroids became visible, resulting in a mixed culture with two different-size populations [Figs. 6(a) and S1(b)]. However, when HPSCs was introduced into culture, this double population was polarized to the smaller one. The growth of the cell clusters formed on day 1 was not affected [Fig. 6(b), BxPC-3]. The p90 area values with and without HPCS were 998.2 and 3330.0, respectively. In contrast, in the case of the other epithelial cell line, Capan-2, we observed a significant increase in the size of the spheroids after coculture with HPSCs [Fig. 6(b), Capan-2], presenting p90 area values of 6850.0 and 3804.0, respectively. For the two cell lines with a more mesenchymal phenotype, Panc-1 and MIA PaCa-2, we observed a very similar exponential growth of spheroid area over time in both culture conditions [Fig. 6(b), Panc-1 and MIA PaCa-2]. A slight increase in the p90 values of MIA PaCa-2 cells was observed in coculture from day 6 onward [Fig. 6(b), MIA PaCa-2]. The p90 area value was 3305.0 for monoculture and 3500.0 in coculture, suggesting a modest increase in the growth potential of larger spheroids under coculture conditions.

To better observe these differences, we closely evaluated the size and morphology of the spheroids obtained from all cell lines at the end point of both conditions. For the BxPC-3 epithelial cell line, there was a greater trend toward the formation of smaller and more circular cell spheroids (median of 368.2 μm^2) compared to spheroids formed in monoculture (median of 1237.0 μm^2) [Figs. 7(b) and 7(c)]. In fact, spheroids larger than 1000 μm^2 were rarely observed in the presence of the HPSCs [Fig. 7(d), BxPC-3]. The percentage population distribution under coculture conditions showed a marked shift toward smaller spheroids, with 80.2% of spheroids being small (<600 μm^2) compared to only 21.2% in monoculture [Fig. 7(d)]. This suggested that the presence of HPSCs significantly inhibits the growth of larger spheroids in BxPC-3, resulting instead in cell clusters with areas similar to those observed in the initial days of the culture [Figs. 6(b) and 7(a)].

In contrast, the Capan-2 cell line exhibited an opposite effect. At the end point, the population of larger spheroids significantly increased under coculture conditions (median 2517.0 μm^2) compared to monoculture (median 1354.0 μm^2) [Fig. 7(b)]. The coculture condition led to a higher proportion of larger and more elongated spheroids

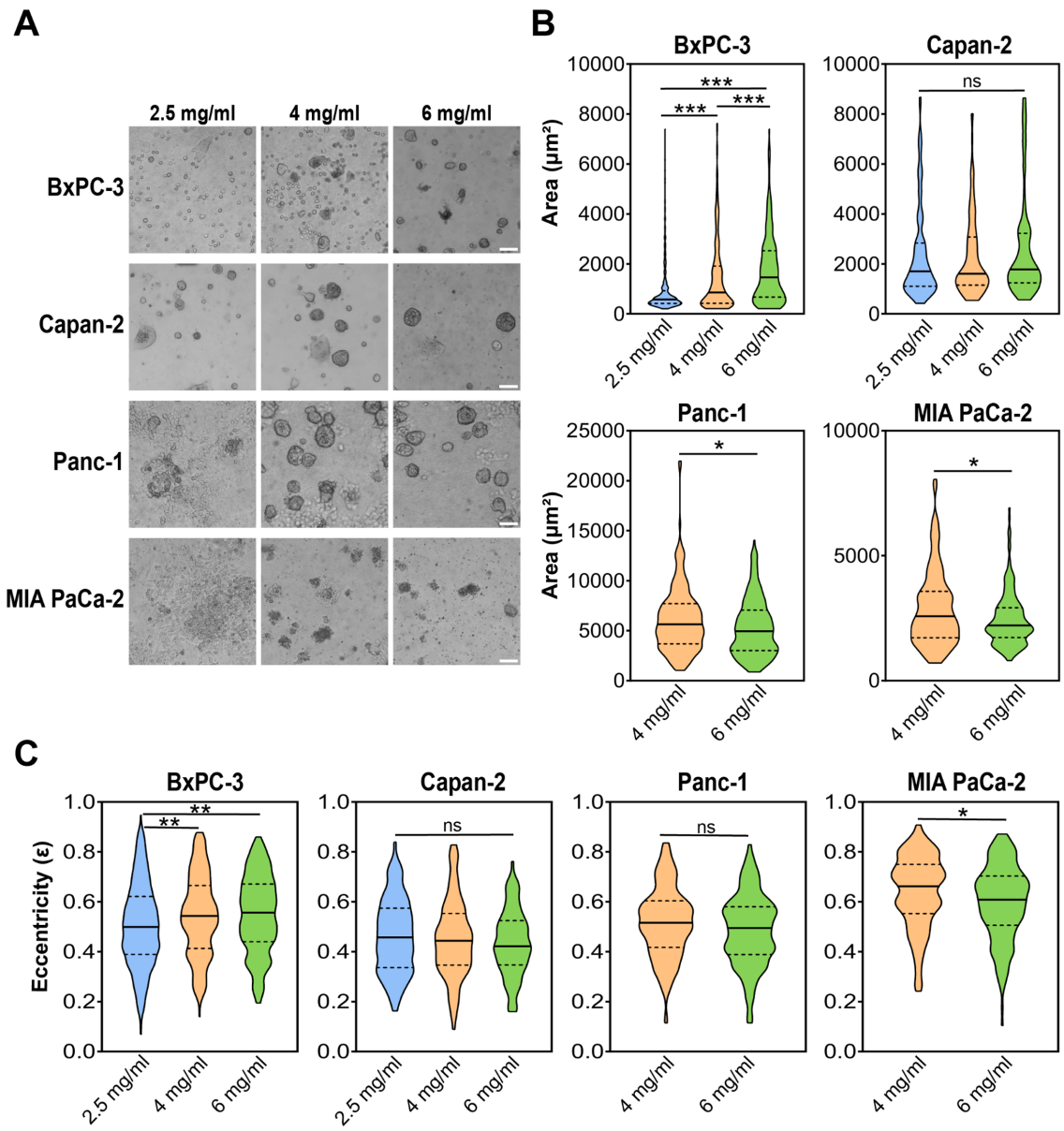

FIG. 3. Quantification of PDAC spheroids in collagen-based matrix at day 10. (a) Brightfield images of PDAC spheroids after 10 days of growth in the indicated collagen matrices (scale bar 100 μm). (b) PDAC spheroids area at day 10 of culture in different collagen concentration hydrogels. (c) Spheroids eccentricity in different collagen matrices at day 10.

[Fig. 7(c), Capan-2]. The percentage population distribution revealed an increase in large (>3000 μm^2) spheroids under coculture conditions, with the proportion increasing from 16.4% in monoculture to 42.5% in coculture [Fig. 7(d)]. This suggested a notable enhancement in spheroid size due to interaction with HPSCs. Nevertheless, in the results obtained for the Panc-1 and MIA PaCa-2 cell lines, we did not observe significant differences in the size or eccentricity of the spheroids formed in both conditions [Figs. 7(b) and 7(c), Panc-1 and MIA PaCa-2]. For the Panc-1 the majority of spheroids remained in the large category (>3000 μm^2) under both conditions, with 77.4% in monoculture and 75.3% in coculture, and in the intermediate size category (600-3000 μm^2) for the MIA PaCa-2 with 85.9% in monoculture and 84.5% in coculture 2 [Fig. 7(d)]. This suggested that the growth dynamics of spheroids for these cell lines are relatively unaffected by HPSCs.

In view of these results, and in order to have a better understanding of the role of the HPSCs in the 3D self-organization process of these cell lines, we made an initial evaluation of the organization of spheroids coculture conditions [Figs. 8(a) and S3(a)]. The data obtained seemed to corroborate the fact that the impact of the HPSCs

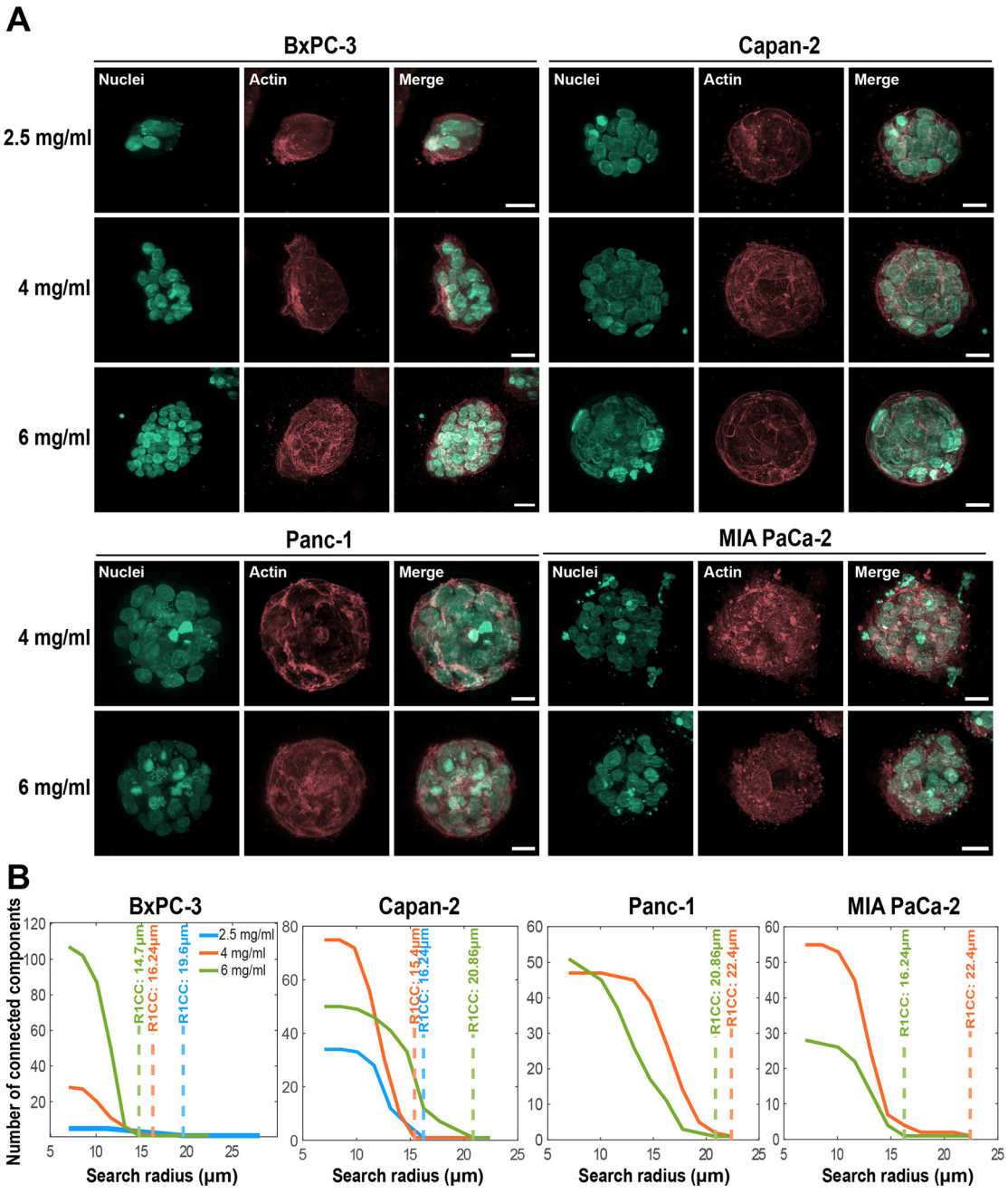

FIG. 4. Cellular organization of PDAC tumor spheroids depending on the mechanical environment given by the difference in collagen concentration of the hydrogel matrices. (a) Fluorescent Lattice Lightsheet (scale bar of 20 μm, 40$\times$ magnification) maximum projection images of the different PDAC cells after 10 days of growth in the indicated collagen matrices. (b) Relationship between the number of connected components and the search radius, reflecting the compactness of the spheroids. The plot indicates the R1CC values, the distance at which all nuclei are connected into a single component.

on PDAC tumor spheroid development appeared to depend on the cellular subtype with which they interact. We found that the presence of the HPSCs appeared to alter the BxPC-3 spheroid organization, resulting in the formation of smaller spheroids with fewer cells (approximately 20) and less intercellular connectivity [Fig. 8(b), BxPC-3]. As we increased the search radius, the number of nuclei connected to form a single object decreased rapidly, with a R1CC of 14.7 μm in comparison with the coculture (R1CC 16.24 μm). However, the average number of cell nuclei neighbors was the same for both conditions, $\approx$4 [Fig. 9(c)]. In the case of the Capan-2 cell line,

we got the opposite result. We found that this cell line contains a higher number of cell nuclei (>60) with higher connectivity (R1CC 19.6) in coculture [Fig. 8(b), Capan-2] comparing with the monoculture condition (50 cells and R1CC value of 20.86 μm). The number of neighbors at R1CC increased from 4 in monoculture to 6 in coculture [Fig. 9(c)]. Therefore, the increase in size [Fig. 7(b)] was likely due to an increase in cell proliferation resulting in spheroids with a higher number of connected cells [Figs. 8 and 9(c)] compared to the monoculture condition.

For the Panc-1 cell line, the spheroids in both conditions appeared to be of similar size [Fig. 7(b)], but in the coculture, we found higher number of cells (≈100) opposed to the monoculture condition (≈50). The radius at which all cell nuclei connect to form a single object was 20.86 μm in the case of monoculture, while it increased slightly to 22.40 μm in the presence of the HPSCs [Fig. 8(b), Panc-1], suggesting a slightly less nuclei connectivity in the presence of the HPSCs. The number of neighbors at R1CC distance also decreased slightly compared to monoculture spheroids [Fig. 9(c)]. Though this effect was not observed in the MIA PaCa-2 cell line. Initially, similar to Panc-1, the presence of the HPSCs resulted in a greater number of cells (>25) in the spheroids generated. However, the nuclei connectivity and the number of neighbors of these spheroids had a similar tendency [Fig. 8(b), MIA PaCa-2 and Fig. 9(c)] with an average distance between cell's nucleus (R1CC) of 16.24 μm for both culture conditions.

Overall, these results demonstrated that the interaction with HPSCs led to cell line-specific effects on spheroid growth dynamics, likely as a consequence of specific molecular signatures and PDAC subtype. In particular, in the presence of HPSCs in the culture, we found inhibition of growth in BxPC-3 cells, enhanced growth for Capan-2, and relatively stable growth patterns for Panc-1 and MIA PaCa-2.

DISCUSSION

PDAC is highly aggressive and characterized by an abundant complex and fibrotic tumor microenvironment,[6,33] primarily composed of ECM and stromal cells, notably CAFs like PSCs.[34] These cells are the main source in the generation of solid stresses and in the deposition of an ECM with altered properties and composition, which contribute to the tumor's progression and immune evasion.[10,35] Given the dynamic nature of the tumor-associated stroma, effective treatments must target both cancer cells and their supportive stromal elements.[13,19] To explore this complexity, we developed a humanized microfluidic 3D model that incorporates key components of the PDAC microenvironment, including collagen I hydrogels (ECM), hPDAC cells, and HPSCs. This system provides quantitative 4D information (3D spatial and temporal evolution of cells) of how tumor cells interact with the microenvironment, specifically with the stromal cells and the surrounding matrix.

We have studied the impact of the matrix collagen concentration on the 3D self-organization of PDAC cells. Previous studies have shown that varying collagen concentration alters the mechanical and microstructural properties of hydrogels regarding the stiffness, pore size, fiber distribution, and permeability,[28,29,38] affecting tumor cell behavior in terms of tumor growth and migration.[35,39–41] Beyond these factors, collagen concentration also significantly influences the rheology of tumor spheroids, affecting their mechanical stability and deformation capacity. Tumor spheroids must adapt to ECM constraints, balancing cell–cell and cell–matrix interactions, which are directly influenced by the viscoelastic properties of the surrounding collagen network.[42,43]

In order to evaluate different PDAC tumor subtypes (classical and squamous/basal-like), we used four human PDAC cell lines with different genetic and molecular profiles.[27] PDAC is a highly heterogeneous cancer, and its classification has evolved from traditional histological grading (G1–G3) to more refined molecular subtypes that impact prognosis and treatment response. The classical subtype cell lines such us Capan-2 and BxPC-3 are characterized by strong epithelial marker expression and generally better clinical outcomes. However, despite both belonging to the classical subtype, BxPC-3 differs from Capan-2 in its degree of histopathological differentiation (G2 vs G1), which may influence its interaction with stromal components. In contrast, Panc-1 and MIA PaCa-2 represent the squamous or basal-like subtype, which exhibits a more mesenchymal markers' expression and is associated with poorer prognosis.[44,45] Understanding these molecular and phenotypic differences is essential when interpreting the variability in tumor–stromal interactions and their impact on *in vitro* models. We have seeded them into Col I hydrogels of varying concentrations (2.5, 4, and 6 mg/ml), leading to the onset and growth of tumor spheroids from single cells within the microfluidic devices (Fig. 1), driven by the biomechanical matrix factors (mainly stiffness and microarchitecture and permeability of the hydrogel matrices) and the cellular activity (mainly tumor cell proliferation and migration). In addition, other cellular actions could occur, such as matrix degradation, production and deposition, and cell contractility. Our approach represents a clear advantage over other 3D culture models that rely on pre-formed multicellular aggregates without an ECM interaction to regulate the spheroid growth.[46–48] Therefore, our strategy is an important step to advance in the understanding of how matrix regulates the morphogenesis of tumor spheroids.

Our results have highlighted the importance of matrix stiffness, microarchitecture, and fluid transport dynamics in regulating tumor spheroid morphogenesis. We have observed differences related to tumor subtype, degree of differentiation, and EMT phenotype among all the analyzed cell lines. Interestingly, classical subtype cells with well-differentiated (Capan-2) and moderately differentiated (BxPC-3) morphology and expression of epithelial markers showed the ability to self-organize into 3D spheroids, regardless of collagen concentration. This ability was not observed in the more mesenchymal phenotype cell lines, Panc-1 and MIA PaCa-2 [Figs. 2(a) and 3(a)], probably due to their migratory capacity. The differences observed in cell behavior according to their classification could suggest that variations in initial cell distribution influenced the results. Specifically, it had to be consider whether differences in cell settling or spatial distribution within the hydrogel could explain the distinct behaviors observed in low (2.5 mg/ml) and high (6 mg/ml) collagen concentrations. To address this, we quantified cell distribution 24 h after the seeding, and confirmed that cell distribution was comparable between low and high collagen concentrations within the same cell line. This analysis revealed that the number of cells in the region that could be in direct contact with the glass surface ($Z \leq 10\ \mu$m) was practically zero across all conditions and cell lines, confirming that sedimentation was not a contributing factor. Cells were predominantly located at greater depths (20–50 μm), reinforcing that they were embedded deeper within the hydrogel rather than in the regions where 2D growth typically occurs [Figs. S5(c) and S5(e)]. The only significant difference in distribution was observed in Panc-1 cells

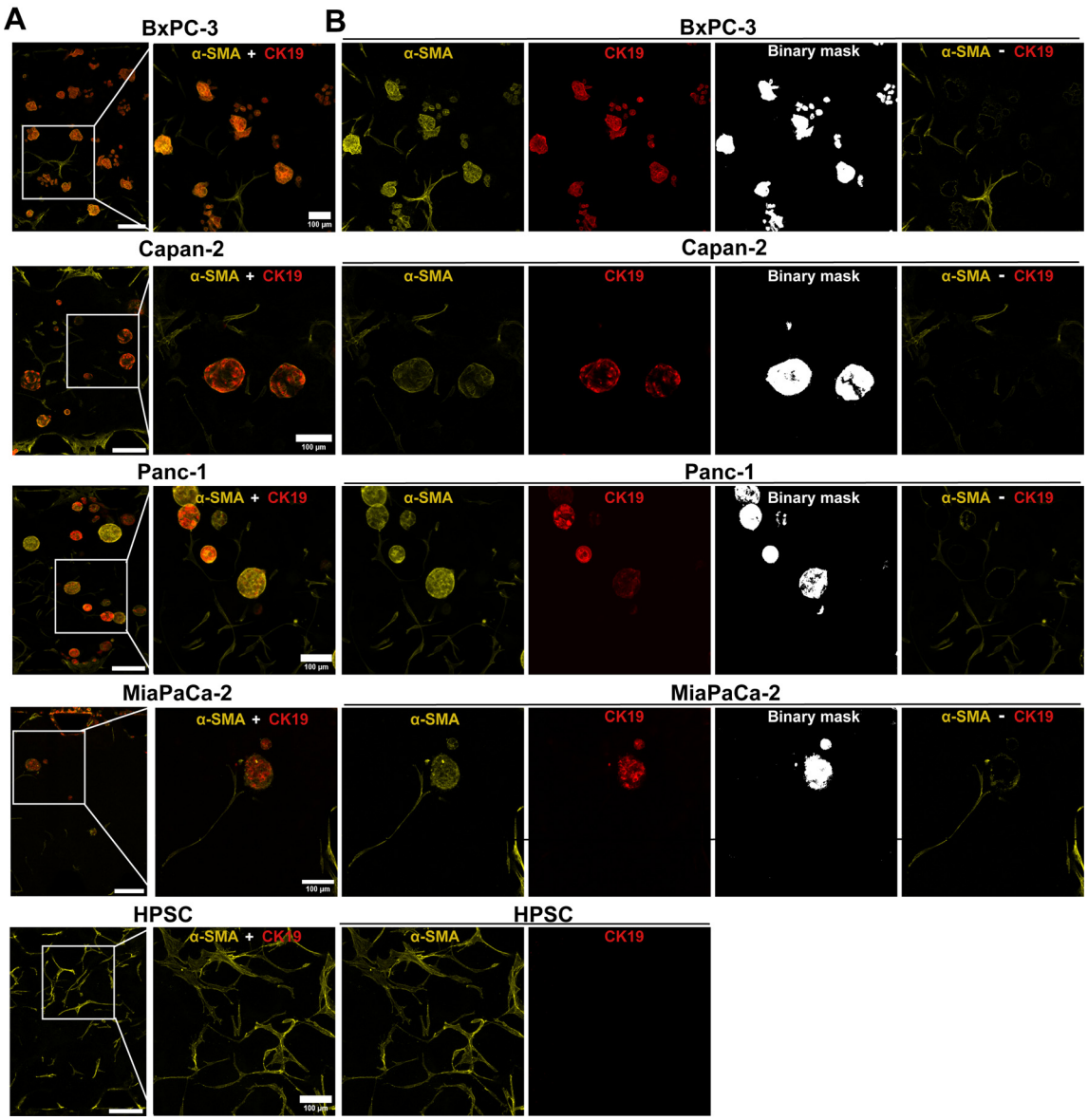

FIG. 5. Immunostaining analysis of HPSCs distribution within the 3D collagen hydrogel after 10 days of culture. (a) Representative fluorescence images showing the distribution of HPSCs and PDAC spheroids. Left: overview of the cocultured cells within the hydrogel (10×, scale bar 200 μm). Right: zoomed-in view illustrating the colocalization of α-SMA (yellow, marking activated HPSCs) and CK19 (red, marking PDAC cells). Scale bar: 100 μm. (b) Colocalization analysis of the HPSCs and PDAC spheroids. Individual fluorescence channels for α-SMA and CK19 are shown separately, followed by the binary CK19 mask used to identify PDAC spheroid structures. The final panel shows the subtraction of the CK19-positive mask from the α-SMA signal, isolating the α-SMA expression of HPSCs from potential tumor-derived α-SMA expression. All fluorescence images represent maximum intensity projections.

in the 6 mg/ml collagen condition, where a greater proportion of cells were found in the 20–50 μm range. [Fig. S5(e)]. However, given that the Panc-1 cells are larger than the other cell lines analyzed, their distribution toward the lower part of the chamber is not surprising. Moreover, this effect was mainly observed in the high-concentration collagen hydrogels (6 mg/ml), where cell growth in 2D was not seen. Importantly, this variation did not affect the critical near-glass region (0–20 μm), confirming that sedimentation did not impact our experimental conditions [Fig. S5(e)]. Additionally, the Alamar Blue assay confirmed that initial cell numbers were comparable across all conditions [Figs. S5(b) and S5(d)]. These findings validated that the observed differences in the spheroid behavior were primarily driven by intrinsic tumor cell properties and their interaction with the ECM, rather than by initial cell distribution within the collagen hydrogel.

To better understand the role of the matrix in this behavior, we characterized the hydraulic permeability of the hydrogels, considering

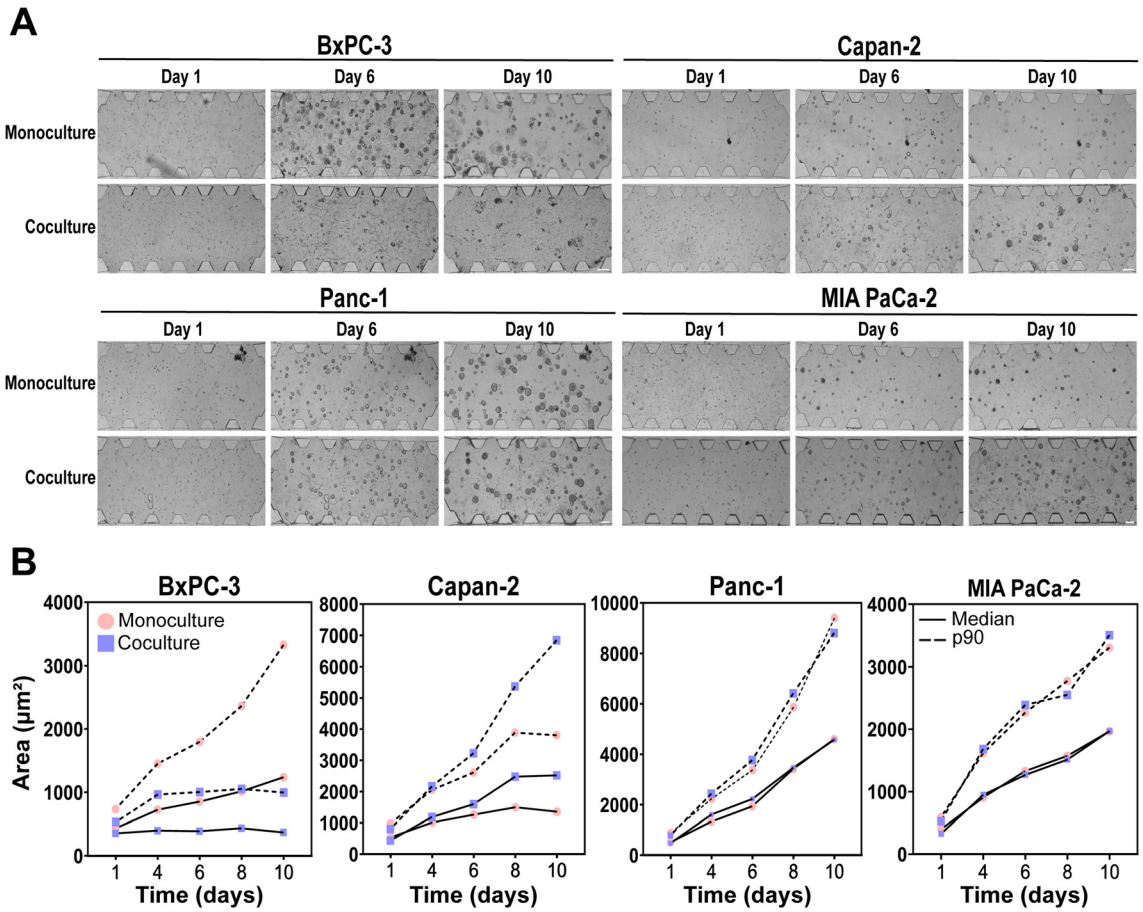

FIG. 6. Growth of PDAC spheroids over time in 6 mg/ml collagen-based matrix with/without HPSCs. (a) Brightfield images of tumor spheroid development over time (up to 10 days) of BxPC-3, Capan-2, Panc-1, and MIA PaCa-2 cell lines in monoculture and coculture with the HPSCs (scale bar 200 μm). (b) Evolution over time of BxPC-3, Capan-2, Panc-1, MIA PaCa-2 spheroid area in monoculture (pink) and coculture (purple). Continuous lines show the median values, and dashed lines represent the 90% percentile (p90) of the different cell lines in each culture condition.

it as a key factor that influences how fluids and soluble factors move through the matrix. While stiffness and microarchitecture are well-established factors in 3D cell behavior, hydraulic permeability may also play a crucial role. Hydraulic permeability, as measured using Darcy's law [Figs. S2(a) and S2(b)], reflects the resistance of the gel to fluid flow, which in turn affects the tumor cell environment. In low-collagen matrices (2.5 mg/ml), the literature emphasizes that the pore size is considerably larger and stiffness is extremely low.[29,39] We observed that the permeability was higher with minimal steric hindrance, allowing easier fluid transport and reducing the physical constraints on cell migration, compared with 4 and 6 mg/ml collagen hydrogels [Figs. S2(c) and S2(d)]. This may facilitate the ability of the more mesenchymal phenotype cell lines to migrate to the lower part of the microfluidic device, adhering to the glass and proliferating there in two dimensions, which is a clear limitation of one approach in gels of low collagen concentration. The formation of spheroid-like structures in these two cell lines was only observed when we increased the collagen concentration of the hydrogels. In contrast to the results obtained in the epithelial spheroids by increasing collagen in the matrix, the spheroids of Panc-1 and MIA PaCa-2 formed in matrices with higher collagen (6 mg/ml) were smaller in size and more regular in shape [Figs. 3(b) and 3(c)], and presented a more nuclei connectivity [Fig. 4(b)] if we compared them with the 4 mg/ml formed spheroids. These cells exhibit reduced cell–cell adhesions and rely more on cell–matrix interactions for migration. The increased fibrillar density and reduced hydraulic permeability [Figs. S2(c) and S2(d)] that increases steric hindrance imposed by narrow pores in the matrix, may be hindering the ability of mesenchymal cells to migrate.[49] Crawford *et al.* described a subdued proliferative response to increase collagen concentration led to a higher cell-ECM friction in 3D tumor breast spheroids that may explain the smaller size of the spheroid observed. This mechanical stress impose for the higher stiffness and the smaller pore size on this type of cells, which are less adapted to such environments compared to epithelial cells, may be inhibiting cell proliferation and spheroid growth, resulting in smaller spheroids.[40,50] In addition to these physical constraints, the effect of ECM viscoelasticity and stress relaxation must also be considered. Elosegui *et al.* demonstrated that tumor spheroids embedded in highly viscoelastic ECMs formed more

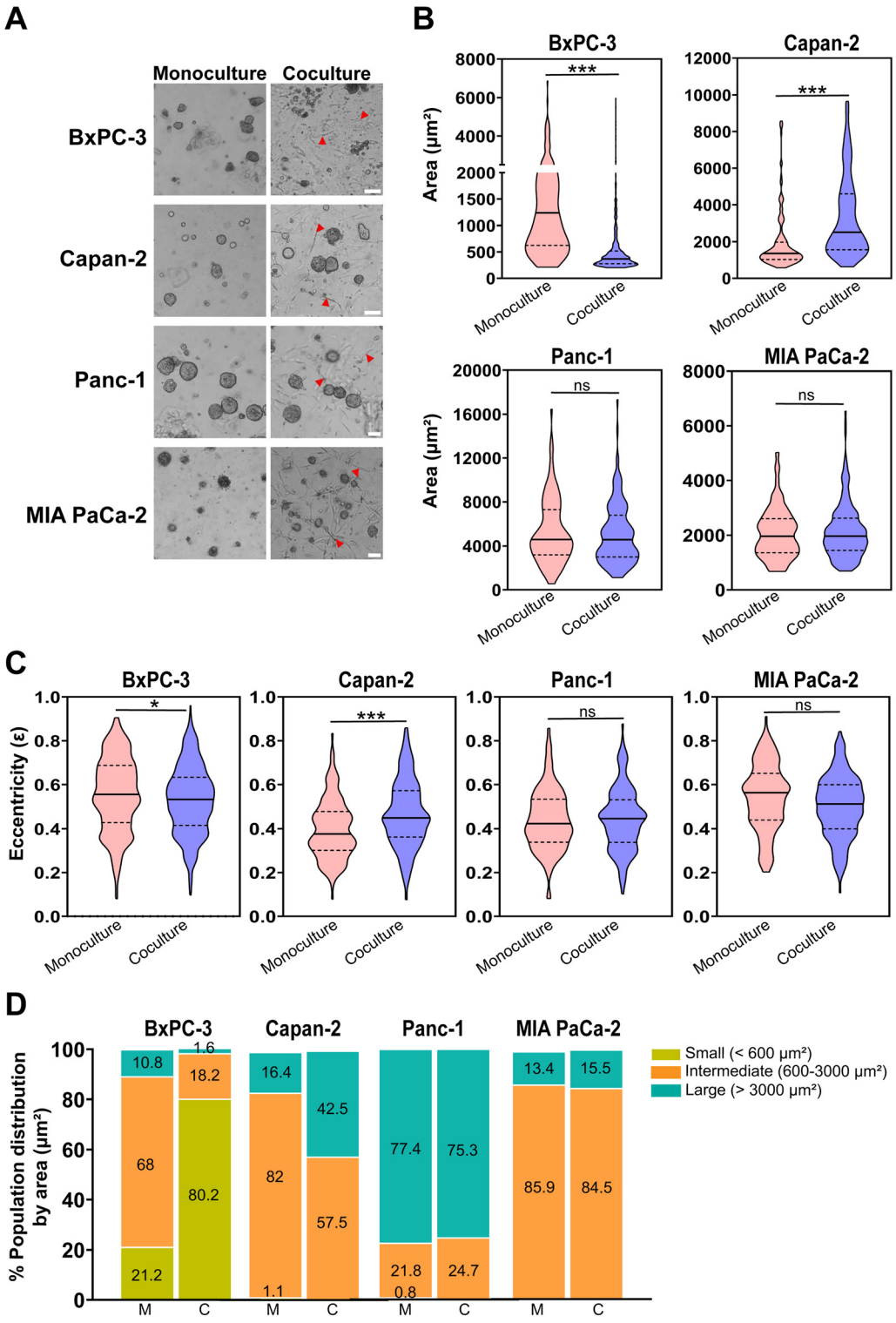

FIG. 7. Characterization of spheroid size and morphology of PDAC cell lines under HSPCs coculture conditions at day 10. (a) Brightfield images of 3D tumor spheroids from the PDAC cell lines at day 10 of culture in the microfluidic devices (scale bar 100 μm). Red arrows point to HPSCs in direct coculture with tumor spheroids. (b) PDAC spheroids area at day 10 of monoculture and coculture. (c) Spheroids eccentricity in monoculture and coculture conditions at day 10. (d) Percentage distribution of spheroid population by area size in monoculture (M) and coculture (C) conditions. Small, intermediate, and large spheroids are represented in green, orange, and blue, respectively.

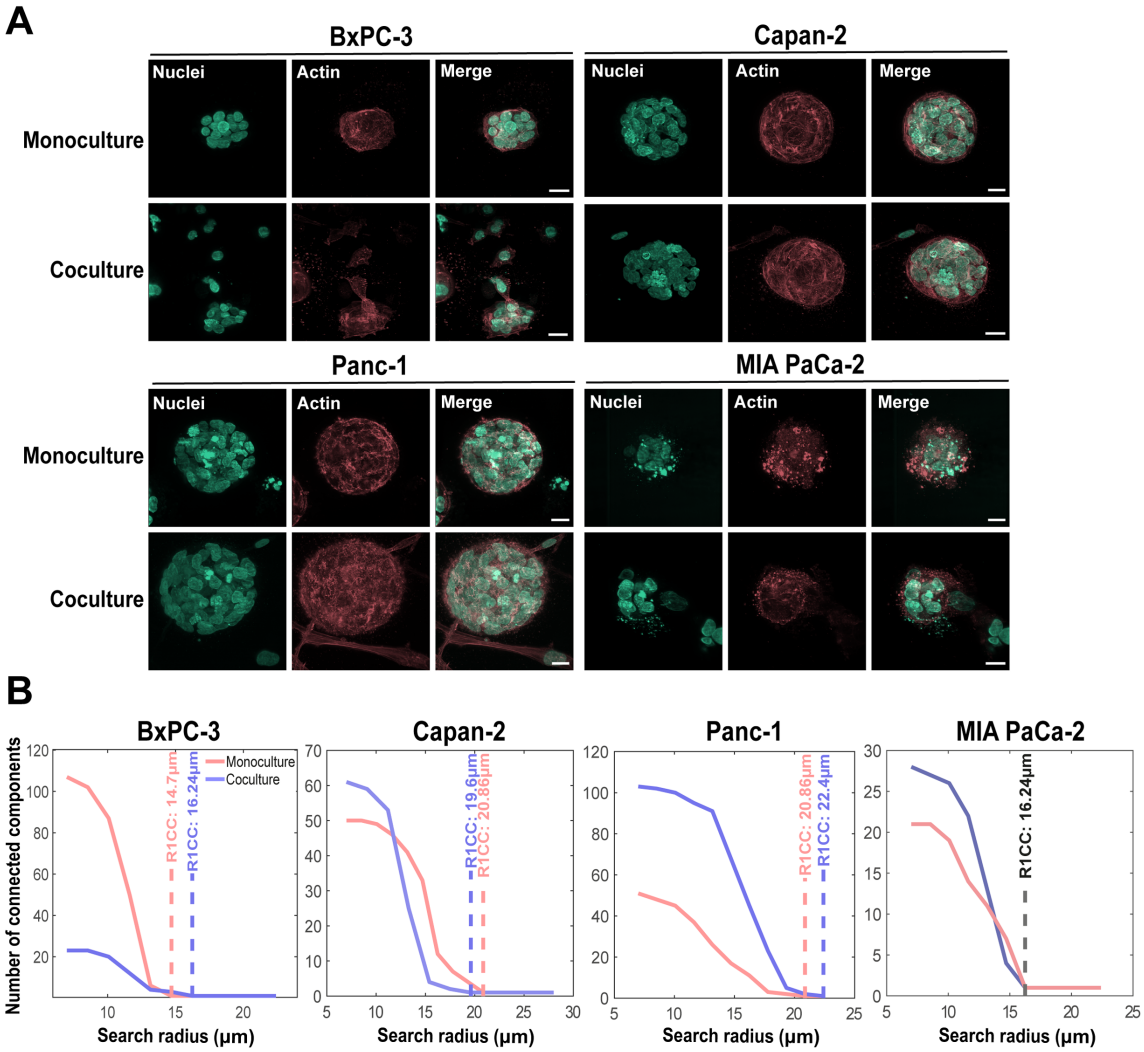

FIG. 8. Cellular organization of PDAC tumor spheroids under monoculture and coculture conditions with HPSCs in 6 mg/ml collagen matrices. (a) Fluorescent Lattice Lightsheet maximum projection images (scale bar of 20 μm, 40× magnification) of the different PDAC cell lines after 10 days of growth under monoculture or coculture conditions. (b) Relationship between the number of connected components and the search radius, reflecting the compactness of the spheroids. The plot indicates the R1CC values, the distance at which all nuclei are connected into a single component.

compact and mechanically reinforced structures, where cell–cell adhesion became dominant over cell–ECM interactions.[42] This aligns with our observations that in denser matrices, mesenchymal spheroids were smaller and more compacted [Figs. 3(a) and 4(b)], suggesting that reduced ECM stress relaxation enhances internal mechanical tension, reinforcing intercellular interactions and limiting spheroid deformability. Furthermore, this slow-relaxing ECM environment found in higher collagen concentrations, reinforce cytoskeletal tension, promoting enhanced nuclear translocation of YAP/TAZ and activating mechanotransduction pathways that contribute to tumor progression.[43] These facts create a more mechanically confined microenvironment, thereby enhancing cell–cell interactions, increasing cytoskeletal tension and reducing single-cell motility. Consequently, these cell types form collective spheroids rather than individual migration [Fig. 3(a)]. In the case of the present study, the observed growth of the tumor spheroids, particularly in the MIA PaCa-2 cell line, may be attributable to a combination of these two factors. First, mechanical confinement that induces a transition to collective migration. Second, an increase in intercellular adhesion that stabilizes the spheroid-like structure.

In general, in the classical cell lines (BxPC-3 and Capan-2), a similar effect was observed in terms of the enhancement of spheroid area growth with increasing collagen concentration. It should be noted, however, that the BxPC-3 spheroids exhibited a greater response to collagen concentration [Figs. 2(c) and 8(a)]. Greater variability and larger spheroid sizes were observed at higher collagen concentrations [Figs. 2(c) and 8(a)], suggesting that higher collagen concentration promotes greater growth in these spheroids, although the response is not uniform. Not all cells respond similarly to the surrounding

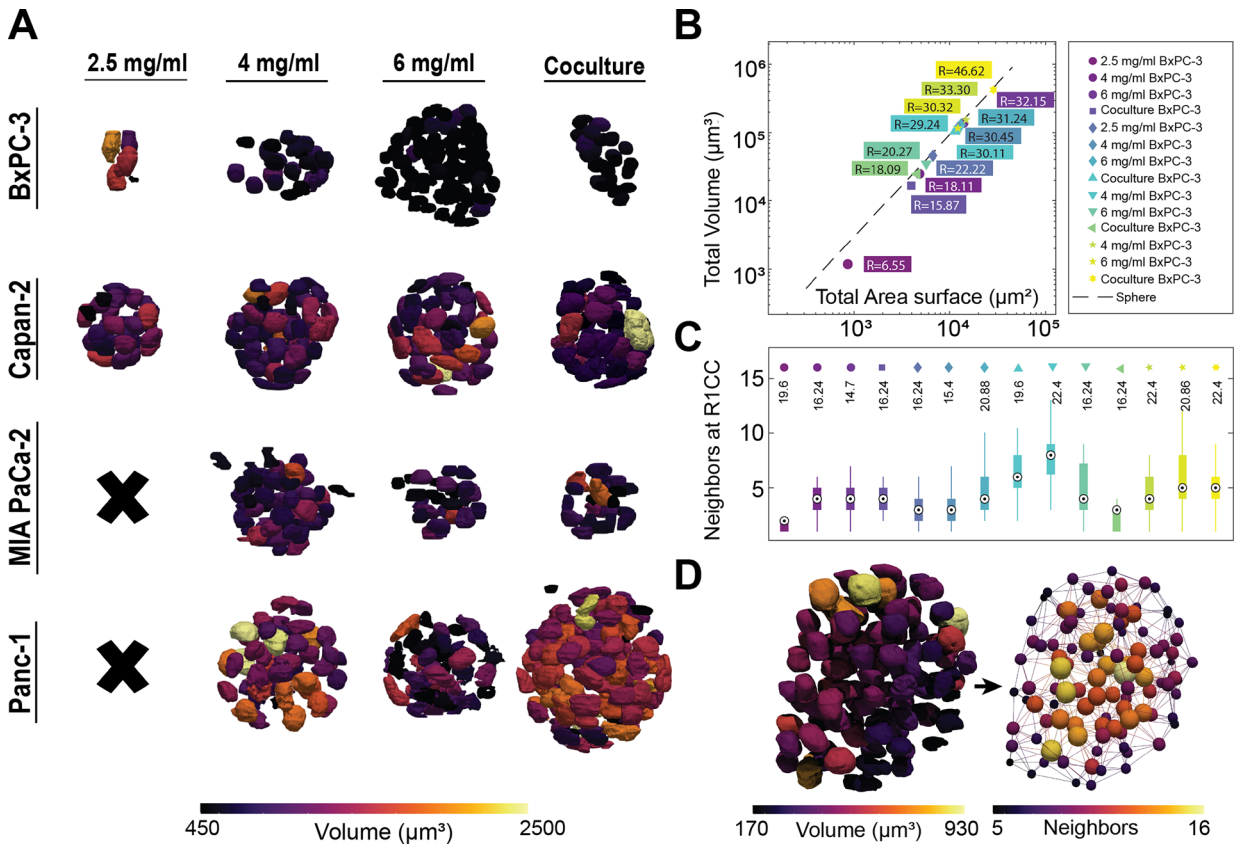

FIG. 9. 3D spheroid organization and analysis across different conditions and cell lines. (a) 3D reconstructions of spheroids for pancreatic cancer cell lines (BxPC-3, Capan-2, MIA PaCa-2, and Panc-1) cultured in collagen hydrogels at different concentrations (2.5, 4, and 6 mg/ml) and under coculture conditions. The color scale represents nuclear volume, ranging from 450 μm^3 (purple) to 2500 μm^3 (yellow). Black crosses indicate non-formation observed. (b) Relationship between the total volume and total surface area of spheroids (measured via their alpha-shape). The diagonal reference line represents the area–volume relationship of a sphere. Labels indicate the radius of an equivalent sphere for each corresponding volume. (c) Number of neighbors for each condition when all nuclei are connected as a single component. Numbers on top of the boxes indicate the search distance (R1CC) at which this occurs. (d) Example 3D visualization of spheroid structures with nuclei color-coded volumes and numbers of neighbors.

mechanical environment. BxPC-3 spheroids also displayed a more irregular shape, indicating a significant influence on both size and shape at higher collagen concentrations [Fig. 3(c)]. These changes have been observed in other types of tumors, such as lung and breast tumors, where there is an increase in the stiffness of the matrix due to an increase in collagen concentration.[35,51] In these tumors, the spheroids formed by the cell lines grew larger and more invasive, and branch-shaped spheroids were observed. It appears that an increase in collagen concentration results in a series of changes in the stiffness and microstructure of the biomimetic hydrogels used, which promote a more aggressive growth and morphology of the epithelial cells.[51,52] However, topographical analysis of the formed spheroids appears to indicate some differences between BxPC-3 and Capan-2. The BxPC-3 spheroids, as well as the mesenchymal PDAC cell lines, had a more connected structure when compared to Capan-2 spheroids at 6 mg/ml matrix [Fig. 4(b)]. It must be noted that changes in collagen concentration affect several ECM properties including elastic modulus, pore size, fiber alignment, and cell speed.[39] These parameters can have different and even opposite effects on spheroid cell organization.

It seems that the observed differences in spheroid formation, growth, and organization among PDAC cell lines with varying collagen concentrations may be attributed to the unique interaction between each cell line and the ECM properties, which influence cellular adaptation to biochemical facts, suggesting differing mechanisms of cell–matrix and cell–cell interactions under the same conditions, which also translates into different downstream consequences. Increasing evidence suggests that the ECM itself is not just a passive scaffold but an active regulator of tumor behavior. In highly fibrotic tumors, cells undergo mechanotransduction-driven adaptations that shape their responses to ECM stiffness and viscoelasticity, influencing proliferation, migration, and overall organization within the matrix.[53] This is consistent with our findings, where changes in collagen concentration resulted in differences in spheroid morphology and organization, suggesting that ECM mechanical properties play a fundamental role in directing tumor cell morphogenesis. One key mechanism through which cells sense and respond to ECM is integrin-mediated adhesion. For instance, alterations in the expression patterns of $\alpha_2\beta_1$ integrin, the principal integrin that interacts with collagen type I, have been observed to modulate adhesion, proliferation, and migration. The

basal-like cell lines analyzed in our study (Panc-1 and MIA PaCa-2) lacked expression of this integrin, whereas in the BxPC-3 line, where it was present, Col I promoted maximum adhesion and proliferation.[54,55] All of this highlights the importance of considering specific receptor–ligand interactions in *in vitro* studies of mechanotransduction to understand how stiffness, composition, and architecture of the ECM act together to regulate cell-specific 3D development.[52,56]

To expand the investigation into the interaction between stromal components and tumor cells beyond the mechanical and structural characteristics of the extracellular matrix in PDAC, we have designed a more complex 3D *in vitro* model. To this aim, another important element of the stroma, α-SMA$^+$ HPSCs, was included in this model. The addition of these cells in their activated state would allow us to partially replicate the interaction between stromal and tumor cells, along with the ECM remodeling dynamics that contribute to the PDAC microenvironment. For this purpose, we have designed a direct coculture system within our microfluidic device, facilitating direct interaction between tumor and stromal cells, as well as direct interaction of both cell types with the ECM. Our model can replicate a real-time physical and biochemical interaction between the two cell populations being examined, within a more physiologically relevant 3D microenvironment. Consequently, it could replace other traditional, less physiological models such as indirect coculture methods that rely on transwell or conditioned-media approaches.[47,57] This advantage holds true even when compared with alternative microfluidic models, where the two cell populations are separated into distinct chambers.[58–60] A key advantage of our model over ULA plates or indirect coculture systems is that HPSCs are distributed within the ECM, rather than forcing their integration into tumor spheroids.[47,57] Immunofluorescence analysis (Fig. 5) confirmed that in our system, α-SMA$^+$ HPSCs remain embedded within the hydrogel, surrounding the tumor spheroids but not becoming part of their structure. This distribution is particularly relevant as it allows HPSCs to actively interact with the matrix, exerting contractile forces and remodeling the ECM. The mechanical influence of HPSCs on the ECM is a critical factor often overlooked in conventional *in vitro* models. While conditioned media approaches capture the paracrine signaling effects of stromal cells, they fail to account for the biomechanical interactions that occur *in vivo*. In our model, the spatial arrangement of HPSCs within the ECM means that their effects on tumor spheroid growth and organization result not only from biochemical signaling but also from mechanical factors. The forces and remodeling processes induced by HPSCs could alter fiber organization and mechanical properties of the hydrogel, ultimately influencing the mechanotransduction pathways of tumor spheroids and modulating their growth dynamics.[61–64] Therefore, our model provides a more comprehensive representation of the PDAC microenvironment, offering a physiologically relevant platform for studying stromal–tumor biochemical and mechanical interactions in 3D.

The coculture engineered was optimized with the objective of achieving a balanced coexistence of the two cell types within the central chamber of our devices, thereby ensuring the viability of the coculture over an extended period of time. By selecting a 2:1 ratio of activated HPSCs to hPDAC cell lines and incorporating both cell types intro high-collagen matrices (6 mg/ml), we have generated a simplified yet more accurate representation of the desmoplastic reaction observed in PDAC tumors, which is primarily driven by PSCs.[12,13] Although we recognize that the PSCs-tumor cell ratios found *in vivo* are typically much higher, this deliberate adjustment allows us to develop an *in vitro* tumor model where the ratio can evolve over time in response to microenvironmental conditions, enabling extended coculture periods.

The differential effects observed across the various PDAC cell lines have highlighted the complexity and cell-specific nature of the stroma–tumor interactions, particularly in the moderate and well-differentiated cell lines (BxPC-3 and Capan-2). We observed a dual effect of the stromal HPSCs in these two PDAC cells. It is well known that pancreatic stromal cells have a positive effect on PDAC progression. In both *in vitro* and *in vivo* models, these cells have been shown to improve tumor growth and promote the migratory and metastatic capacity of tumor cells.[34,59,65] Both of these effects have been observed in our model, but distinctively depending on the cell type. HPSCs may secrete growth factors and cytokines[66,67] that may influence cell–cell adhesion, growth, proliferation, and migration differently in these cell lines. The presence of this stromal cells with Capan-2 cells led to a significant increase in both the median and p90 values of spheroid size, spherical morphology [Fig. 7(c)], and nuclear connectivity (Fig. 8), suggesting a stimulatory effect of HPSCs on Capan-2 growth [Fig. 6(b)] that promotes a more regular and cohesive cellular organization within Capan-2 spheroids. Interestingly, when HPSCs were introduced into the collagen matrix, they had opposite effects, significantly inhibited the formation of larger spheroid structures by BxPC-3 cells. This effect was supported by statistical data showing lower median and p90 values in coculture, indicating reduced capacity for spheroid enlargement [Fig. 6(b)]. Moreover, the presence of HPSCs led to a polarization toward smaller, less spherical [Figs. 7(b) and 7(c)] and less connected cell spheroids (Fig. 8), suggesting that HPSCs might be altering spheroid proliferation, formation, and integrity in this PDAC cell line. The BxPC-3 line appeared to be more sensitive to growth inhibitory or EMT and migratory signals. The less connected structures observed in coculture in the BxPC-3 line might be due to a loss of tight junctions, a characteristic feature of the EMT process.[68] HPSCs may act as EMT effectors, shifting toward more invasive and mesenchymal phenotypes. In other coculture models, this phenomenon has also been seen in a cell line-specific manner, with a decrease in epithelial markers like E-cadherin and an increase in mesenchymal markers such as vimentin.[59,69] Moreover, proliferation-inhibiting effect appears to be related to EMT stimulation by CAFs in coculture.[67,70] Regarding the role of CAFs in the proliferation, recent studies have elucidated their key role in tumor cell proliferation by modulating mechanotransduction through YAP, which may also explain the effect observed in the BxPC-3 cell line. It has been shown that CAFs present in other solid tumors generate a capsule, formed by excessive ECM production, which actively compresses tumor cells. This force leads to changes in the localization of the transcriptional regulator YAP, possibly resulting in decreased proliferation rates.[71]

Nevertheless, we have observed the distinct responses of PDAC cell lines when they grew under matrices with similar properties. PSCs are known to actively participate in matrix deposition and remodeling processes.[72] Other studies have shown their ability to modify the fiber alignment and pore size of collagen matrices.[64,66,73] This modification of some biomechanical properties by HPSC activity may impact the growth and organization of PDAC cell spheroids differently, as indicated in the analysis of collagen concentration effects. Studies have shown the importance of the orientation of Col I fibers in the

progression and metastasis of cancer.[64,74] Further research on coculture matrix properties and composition is necessary to determine HPSC's effect on mechanical properties of hydrogels in our model, and to establish a potential correlation between differences in 3D cell lines growth and property modifications in monoculture vs coculture conditions. These results have demonstrated a differential effect of HPSCs on spheroid formation and growth in these two PDAC cell lines, possibly attributed to genetic or phenotypic differences in these cells, which make their interaction with HPSCs mediated by cell-specific signaling pathways or ECM remodeling processes. Interestingly, the BxPC-3 cell line lacks one of the most common KRAS gene mutations found in PDAC. This differential feature, given that the KRAS mutation is a key driver of this disease, could potentially contribute to the distinctly different effects we have observed in its interaction with the HPSCs stromal cell line, particularly in comparison with the Capan-2 well-differentiated epithelial cell line.[27,75]

It should be emphasized that the coculture effect observed on the mesenchymal-like Panc-1 and MIA PaCa-2 cell lines has not been so relevant. They showed similar growth patterns of spheroids in both monoculture and coculture conditions [Fig. 6(b)]. It is true that MIA PaCa-2 spheroids seemed to show a modest increase in p90 values in coculture, indicating a slight enhancement in the growth potential of larger spheroids [Fig. 6(b)] and a slightly more regular morphology [Fig. 7(c)]. The observation that no significant effect of coculture was observed in these cell lines may be due to the cells having lost their differentiation to a greater degree, and they already have a more aggressive capacity in terms of proliferation and migration. The role of the stroma in PDAC remains highly controversial. While some studies suggest a protective role for HPSCs, containing tumor cells, others emphasize their pro-tumoral effects, favoring tumor growth and increased aggressiveness.[76–78] This dual nature could be observed in our model when comparing epithelial and mesenchymal PDAC cells. The different cell lines studied may secrete factors that differentially impact the activity of the stromal HPSCs, leading to variable effects on each tumor subtype. In the case of epithelial lines, we may observe a more malignant role, where the interaction with the HPSCs promotes greater growth (Capan-2 cells), metastatic capacity, and tumor progression (BxPC-3 cells). Conversely, in the mesenchymal lines (Panc-1 and MIA PaCa-2), we may see a protective role of the stroma, containing these more aggressive tumor cells.

These findings highlight the importance of the ECM's properties and the HPSCs role in influencing the growth and organization of tumor spheroids. They suggest that PDAC's cell-specific differences (genetic and phenotypic) mark a unique response to changes in matrix mechanical and structural characteristics, as well as to direct interaction with other stromal cell types such as HPSCs. This could have significant implications, optimizing the growth conditions for different tumor cell lines, potentially enhancing the efficacy of *in vitro* tumor models and leading to more accurate predictions of *in vivo* behavior.

To better understand the translational relevance of our findings, it is important to compare them with more complex PDAC preclinical models, such as patient-derived organoids and *in vivo* models. These systems provide a broader representation of PDAC progression, capturing the full heterogeneity and complexity of the tumor microenvironment. Organoid models have emerged as powerful *ex vivo* platforms to study PDAC biology, as they preserve genetic heterogeneity, tumor architecture, and microenvironmental responses.[79] Studies have demonstrated that PDAC organoids exhibit distinct morphological and phenotypic traits depending on their genetic background and ECM interactions.[80] Additionally, branched organoid models have shown that intratumoral heterogeneity and epithelial-to-mesenchymal plasticity are strongly influenced by ECM composition and mechanical constraints.[81] These findings illustrate the complex role of PDAC desmoplasia, showing that collagen properties may influence tumor progression.

Beyond organoids, *in vivo* models provide a more comprehensive representation of PDAC progression, as they include tumor–stroma interactions, immune responses, vascularization, and progressive ECM remodeling.[82] In these models, increased collagen deposition has been correlated with enhanced tumor stiffness, impaired drug penetration, and altered invasion patterns, primarily due to the influence of CAFs and activated PSCs.[7,14] Furthermore, studies by Hwang *et al.* and Orozco *et al.* have demonstrated the key role of HPSCs in modulating PDAC progression. Hwang *et al.* used xenografts to show that HPSCs promote tumor growth, enhance invasion, and contribute to chemoresistance. Tumors co-injected with the HPSCs exhibited larger sizes and altered structural organization.[34] Their findings align with our results, as we observed that HPSCs coculture significantly influenced the growth and morphology of tumor spheroids, reinforcing the concept that PSCs actively shape tumor architecture through biochemical and mechanical interactions. Similarly, Orozco *et al.* investigated the role of depleting galectin-1 (a stromal-derived glycan-binding protein) in PSCs on tumor development. Orthotopic co-injection with BxPC-3 pancreatic tumor cells demonstrated that depletion of Galectin-1 in HPSCs reduces tumor size, angiogenesis, stroma activation, and metastasis.[36] Their findings emphasize the importance of the stromal microenvironment in determining PDAC progression.

These insights are also supported with our study by showing that PDAC tumor cells dynamically adapt their growth and 3D organization based on surrounding stromal cues such collagen concentration and HPSCs' presence. Despite, *in vivo* and patient-derived *in vitro* cultures represent a more physiologically complex model with intricate tissue-like organization, our system offers a distinct advantage through the precise control and real-time quantification of tumor structural responses to the impact of specific key stromal components of the PDAC microenvironment. This makes our approach particularly valuable for investigating the biomechanical characteristics and the influence of stromal cell lines on the patterns of cellular growth, morphology, and organization for each PDAC subtype. While our microfluidic tumor model presents significant advantages in studying stroma-driven tumor behavior, it is crucial to consider some current limitations in order to delineate the underlying biological mechanism behind our results. *In vivo* models provide a more comprehensive representation of PDAC progression, including immune-tumor interactions and vascular contributions, which our system does not yet integrate. Likewise, organoid models capture the heterogeneity and cellular complexity of PDAC, making them the ideal system for studying tumor evolution and treatment responses over time. Therefore, our efforts are currently being directed at using our platform to develop more complex patient-derived models that better recapitulate the heterogeneity of PDAC, which will be reflected in future publications. Importantly, we must emphasize that the controlled microenvironment and real-time monitoring capabilities of the system presented in this work provide a valuable framework to refine and optimize these

advanced models, offering a complementary approach to dissect the mechanical and structural influences of the stroma on tumor growth.

All the results observed in our study pave the way for future research to deepen into the exact mechanisms underlying the observed effects. Elucidating the precise mechanism by which specific ECM components and stromal cells modulate tumor cell behavior and outcomes, will not only enhance our comprehension of PDAC progression, but also contribute to the development of novel therapeutic strategies and diagnostic approaches. Our future efforts will focus on overcoming current limitations to enable more detailed mechanistic studies at the molecular level.

CONCLUSIONS

We have developed a simplified and validated novel 3D microfluidic-based model that allows the study of tumor–stroma interaction. The findings of the study have demonstrated the complex cell line-specific interplay between pancreatic ductal adenocarcinoma (PDAC) cell lines, human pancreatic stellate cells (HPSCs), and collagen matrix characteristics, pointing to the importance of these components in tumor microenvironment interactions. Our results have demonstrated that variation in the concentration of collagen present in the extracellular matrix (ECM) critically and differently affects the growth patterns and architectural organization of PDAC cell spheroids depending on the tumor subtype and its epithelial–mesenchymal phenotypes. We observed that increasing collagen concentration in the biomimetic matrix promotes the growth of larger spheroids in lines with more epithelial characteristics. While this increase is necessary for mesenchymal cells to self-organize into spheroids, these spheroids are smaller compared to those in lower collagen matrices. These changes were associated with alterations in the mechanical properties of the hydrogels, particularly in terms of stiffness, microstructure, and hydraulic permeability. Similarly, the presence and interaction with stromal HPSCs profoundly influenced the formation of PDAC spheroids in our microfluidic devices. The differences appeared to be dependent on the unique genetic and phenotypic characteristics of each PDAC cell line. Only in the spheroids of the more epithelial-like cell lines was an opposite effect of the stromal cells observed.

Our work highlights the key role that the matrix plays in the morphogenesis of the tumor spheroid, depending on the characteristics of each cell within the tumor, and other conditions such as the presence of other stromal cell types present in the tumor. These findings open avenues for further investigation to unravel the precise molecular pathways and cellular interactions mediating these effects. Our model should facilitate the study of further insights of tumor-stroma 3D crosstalk, and it opens the door to the generation of other more complex but more physiopathological models of human PDAC, which are already ongoing in our laboratory. These models will incorporate other stromal cell types in a 3D microenvironment formed by more components of the ECM, which will allow a more exhaustive study of the PDAC tumor microenvironment and will allow us to advance in the development of new therapeutic strategies for PDAC.

SUPPLEMENTARY MATERIAL

See the supplementary material for additional tables and figures to support the findings presented in the manuscript. Tables SI–S3 provide approximate values for the mean diameters and areas of individual PDAC cells, as well as median and p90 values of spheroid area (μm^2) over time under various culture conditions. Figures S1–S5 illustrate the evolution of spheroid growth area over a 10-day period in collagen-based microfluidic devices, the quantification of permeability in type I collagen hydrogels through Darcy's Law, a visualization of the search process to achieve a single connected component in the analysis of cellular nuclei, the viability of the PDAC spheroids in the high-collagen hydrogel (6 mg/ml) within the microfluidic device and cell distribution analysis after the hydrogel polymerization, respectively. In addition, the methods section shows the protocols followed for the experimental work presented in these figures.

ACKNOWLEDGMENTS

This work is part of the project PID2021-122409OB-C21 funded by MCINN/AEI/10.13039/501100011033/FEDER, UE. The authors would like to acknowledge the European Research Council (ERC) under the EU's Horizon 2020 programme (ICoMICs, G.A.nr. 101018587) (J.M.G.A.), the MICINN/ Instituto de Salud Carlos III (ISCIII)-FEDER (Grant No. PI20/00625 and PI23/00591) (P.N.), the FJC2021-048046-I funded MCINN/AEI/ and the EU "NextGenerationEU"/PRTR" (P.E.G), and the pre-doctoral grants for the training of doctors funded by the MICINN (PRE2019-090264) (S.H.H).

We would like to thank María del Valle Blázquez-Romero from the I3A, University of Zaragoza for their assistance in coding the custom MATLAB script for the cell distribution analysis.

AUTHOR DECLARATIONS

Conflict of Interest

The authors have no conflicts to disclose.

Ethics approval

Ethics approval is not required.

Author Contributions

Soraya Hernández-Hatibi: Conceptualization (equal); Data curation (lead); Formal analysis (lead); Investigation (lead); Methodology (lead); Validation (lead); Writing – original draft (lead). **Carlos Borau:** Data curation (lead); Formal analysis (lead); Software (lead); Writing – review & editing (equal). **Neus Martínez-Bosch:** Methodology (supporting); Resources (supporting); Writing – review & editing (equal). **Pilar Navarro:** Methodology (supporting); Resources (supporting); Writing – review & editing (equal). **Jose Manuel García-Aznar:** Conceptualization (equal); Funding acquisition (lead); Project administration (lead); Resources (lead); Supervision (lead); Writing – review & editing (equal). **Pedro Enrique Guerrero:** Conceptualization (equal); Project administration (supporting); Supervision (lead); Validation (equal); Writing – review & editing (equal).

DATA AVAILABILITY

The data that support the findings of this study are available from the corresponding author upon reasonable request.

REFERENCES

[1]P. Rawla, T. Sunkara, and V. Gaduputi, "Epidemiology of pancreatic cancer: Global trends, etiology and risk factors," World J. Oncol. **10**(1), 10–27 (2019).

[2]R. L. Siegel, A. N. Giaquinto, and A. Jemal, "Cancer statistics, 2024," CA-Cancer J. Clin. **74**(1), 12–49 (2024).
[3]Á. Sally, R. McGowan, K. Finn, and B. M. Moran, "Current and future therapies for pancreatic ductal adenocarcinoma," Cancers **14**(10), 2417 (2022).
[4]R. S. Ahmad, T. D. Eubank, S. Lukomski, and B. A. Boone, "Immune cell modulation of the extracellular matrix contributes to the pathogenesis of pancreatic cancer," Biomolecules **11**(6), 901 (2021).
[5]K. J. Murphy, C. R. Chambers, D. Herrmann, P. Timpson, and B. A. Pereira, "Dynamic stromal alterations influence tumour-stroma crosstalk to promote pancreatic cancer and treatment resistance," Cancers **13**(14), 3481 (2021).
[6]E. Hessmann *et al.*, "Microenvironmental determinants of pancreatic cancer," Physiol. Rev. **100**(4), 1707–1751 (2020).
[7]A. Neesse *et al.*, "Stromal biology and therapy in pancreatic cancer: Ready for clinical translation?," Gut **68**(1), 159–171 (2019).
[8]M. H. Sherman and G. L. Beatty, "Tumour microenvironment in pancreatic cancer pathogenesis and therapeutic resistance," Annu. Rev. Pathol. **18**(1), 123–148 (2023).
[9]C. Tian *et al.*, "Proteomic analyses of ECM during pancreatic ductal adenocarcinoma progression reveal different contributions by tumour and stromal cells," Proc. Natl. Acad. Sci. U. S. A. **116**(39), 19609 (2019).
[10]L. N. C. Boyd, K. D. Andini, G. J. Peters, G. Kazemier, and E. Giovannetti, "Heterogeneity and plasticity of cancer-associated fibroblasts in the pancreatic tumour microenvironment," Semin. Cancer Biol. **82**, 184–196 (2022).
[11]M. Erkan *et al.*, "StellaTUM: Current consensus and discussion on pancreatic stellate cell research," Gut **61**(2), 172–178 (2012).
[12]V. M. Perez, J. F. Kearney, and J. J. Yeh, "The PDAC extracellular matrix: A review of the ECM protein composition, tumour cell interaction, and therapeutic strategies," Front. Oncol. **11**, 751311 (2021).
[13]Y. Wu, C. Zhang, K. Jiang, J. Werner, A. V. Bazhin, and J. G. D'Haese, "The role of stellate cells in pancreatic ductal adenocarcinoma: Targeting perspectives," Front. Oncol. **10**, 621937 (2021).
[14]P. P. Provenzano, C. Cuevas, A. E. Chang, V. K. Goel, D. D. Von Hoff, and S. R. Hingorani, "Enzymatic targeting of the stroma ablates physical barriers to treatment of pancreatic ductal adenocarcinoma," Cancer Cell **21**(3), 418–429 (2012).
[15]E. Henke, R. Nandigama, and S. Ergün, "Extracellular matrix in the tumour microenvironment and its impact on cancer therapy," Front. Mol. Biosci. **6**, 160 (2020).
[16]D. Wang, Y. Li, H. Ge, T. Ghadban, M. Reeh, and C. Güngör, "The extracellular matrix: A key accomplice of cancer stem cell migration, metastasis formation, and drug resistance in PDAC," Cancers **14**(16), 3998 (2022).
[17]B. Farran and G. P. Nagaraju, "The dynamic interactions between the stroma, pancreatic stellate cells and pancreatic tumour development: Novel therapeutic targets," Cytokine Growth Factor Rev. **48**, 11–23 (2019).
[18]Y. Li, J. Wang, H. Wang, S. Zhang, Y. Wei, and S. Liu, "The interplay between inflammation and stromal components in pancreatic cancer," Front. Immunol. **13**, 850093 (2022).
[19]W. J. Ho, E. M. Jaffee, and L. Zheng, "The tumour microenvironment in pancreatic cancer—clinical challenges and opportunities," Nat. Rev. Clin. Oncol. **17**(9), 527 (2020).
[20]F. Polani, P. M. Grierson, and K.-H. Lim, "Stroma-targeting strategies in pancreatic cancer: Past lessons, challenges and prospects," World J. Gastroenterol. **27**(18), 2105–2121 (2021).
[21]P. Datta, M. Dey, Z. Ataie, D. Unutmaz, and I. T. Ozbolat, "3D bioprinting for reconstituting the cancer microenvironment," npj Precis. Oncol. **4**(1), 18 (2020).
[22]O. Habanjar, M. Diab-Assaf, F. Caldefie-Chezet, and L. Delort, "3D cell culture systems: Tumour application, advantages, and disadvantages," Int. J. Mol. Sci. **22**(22), 12200 (2021).
[23]A. M. K. Law, L. Rodriguez de la Fuente, T. J. Grundy, G. Fang, F. Valdes-Mora, and D. Gallego-Ortega, "Advancements in 3D cell culture systems for personalizing anti-cancer therapies," Front. Oncol. **11**, 782766 (2021).
[24]Y. Shin *et al.*, "Microfluidic assay for simultaneous culture of multiple cell types on surfaces or within hydrogels," Nat. Protoc. **7**(7), 1247 (2012).
[25]A. Sontheimer-Phelps, B. A. Hassell, and D. E. Ingber, "Modelling cancer in microfluidic human organs-on-chips," Nat. Rev. Cancer **19**(2), 65 (2019).
[26]C. Li, J. B. Holman, Z. Shi, B. Qiu, and W. Ding, "On-chip modeling of tumour evolution: Advances, challenges and opportunities," Mater. Today Bio **21**, 100724 (2023).
[27]E. L. Deer *et al.*, "Phenotype and genotype of pancreatic cancer cell lines," Pancreas **39**(4), 425–435 (2010).
[28]V. Olivares, M. Cóndor, C. Del Amo, J. Asín, C. Borau, and J. M. García-Aznar, "Image-based characterization of 3D collagen networks and the effect of embedded cells," Microsc. Microanal. **25**(4), 971–981 (2019).
[29]C. Valero, H. Amaveda, M. Mora, and J. M. García-Aznar, "Combined experimental and computational characterization of crosslinked collagen-based hydrogels," PLoS One **13**(4), e0195820 (2018).
[30]W. A. Farahat *et al.*, "Ensemble analysis of angiogenic growth in three-dimensional microfluidic cell cultures," PLoS One **7**(5), e37333 (2012).
[31]S. Hernández-Hatibi, P. E. Guerrero, J. M. García-Aznar, and E. García-Gareta, "Polydopamine interfacial coating for stable tumour-on-a-chip models: Application for pancreatic ductal adenocarcinoma," Biomacromolecules **25**(8), 5169–5180 (2024).
[32]P. M. Schmidtlein *et al.*, "A comparative endocrine trans-differentiation approach to pancreatic ductal adenocarcinoma cells with different EMT phenotypes identifies quasi-mesenchymal tumour cells as those with highest plasticity," Cancers **13**(18), 4663 (2021).
[33]F. Minami *et al.*, "Morphofunctional analysis of human pancreatic cancer cell lines in 2- and 3-dimensional cultures," Sci. Rep. **11**(1), 6775 (2021).
[34]R. F. Hwang *et al.*, "Cancer-associated stromal fibroblasts promote pancreatic tumour progression," Cancer Res. **68**, 918–926 (2008).
[35]J. Plou, Y. Juste-Lanas, V. Olivares, C. del Amo, C. Borau, and J. M. García-Aznar, "From individual to collective 3D cancer dissemination: Roles of collagen concentration and TGF-β," Sci. Rep. **8**(1), 12723 (2018).
[36]C. A. Orozco *et al.*, "Targeting galectin-1 inhibits pancreatic cancer progression by modulating tumour–stroma crosstalk," Proc. Natl. Acad. Sci. U. S. A. **115**, E3769–E3778 (2018).
[37]E. Ryschich, A. Khamidjanov, V. Kerkadze, M. W. Büchler, M. Zöller, and J. Schmidt, "Promotion of tumour cell migration by extracellular matrix proteins in human pancreatic cancer," Pancreas **38**(7), 804–810 (2009).
[38]T. Kulkarni, O.-M. Robinson, A. Dutta, D. Mukhopadhyay, and S. Bhattacharya, "Machine learning-based approach for automated classification of cell and extracellular matrix using nanomechanical properties," Mater. Today Bio **25**, 100970 (2024).
[39]S. I. Fraley *et al.*, "Three-dimensional matrix fiber alignment modulates cell migration and MT1-MMP utility by spatially and temporally directing protrusions," Sci. Rep. **5**(1), 14580 (2015).
[40]I. G. Gonçalves and J. M. Garcia-Aznar, "Extracellular matrix density regulates the formation of tumour spheroids through cell migration," PLoS Comput. Biol. **17**(2), e1008764 (2021).
[41]P. Alamán-Díez *et al.*, "Collagen-Laponite nanoclay hydrogels for tumour spheroid growth," Biomacromolecules **24**(6), 2879–2891 (2023).
[42]A. Elosegui-Artola *et al.*, "Matrix viscoelasticity controls spatiotemporal tissue organization," Nat. Mater. **22**(1), 117–127 (2023).
[43]H. D. Nguyen and C.-C. Lin, "Viscoelastic stiffening of gelatin hydrogels for dynamic culture of pancreatic cancer spheroids," Acta Biomater. **177**, 203–215 (2024).
[44]S. N. Kalimuthu *et al.*, "Morphological classification of pancreatic ductal adenocarcinoma that predicts molecular subtypes and correlates with clinical outcome," Gut **69**(2), 317–328 (2020).
[45]R. A. Moffitt *et al.*, "Virtual microdissection identifies distinct tumour- and stroma-specific subtypes of pancreatic ductal adenocarcinoma," Nat. Genet. **47**(10), 1168–1178 (2015).
[46]S. Nath and G. R. Devi, "Three-dimensional culture systems in cancer research: Focus on tumour spheroid model," Pharmacol. Ther. **163**, 94–108 (2016).
[47]K. J. Norberg *et al.*, "A novel pancreatic tumour and stellate cell 3D coculture spheroid model," BMC Cancer **20**(1), 475 (2020).
[48]G. Lazzari, V. Nicolas, M. Matsusaki, M. Akashi, P. Couvreur, and S. Mura, "Multicellular spheroid based on a triple coculture: A novel 3D model to mimic pancreatic tumour complexity," Acta Biomater. **78**, 296–307 (2018).
[49]F. Merino-Casallo, M. J. Gomez-Benito, R. Martinez-Cantin, and J. M. Garcia-Aznar, "A mechanistic protrusive-based model for 3D cell migration," Eur. J. Cell Biol. **101**(3), 151255 (2022).
[50]A. J. Crawford *et al.*, "Tumour proliferation and invasion are intrinsically coupled and unraveled through tunable spheroid and physics-based models," Acta Biomater. **175**, 170–185 (2024).

[51]M. J. Paszek *et al.*, "Tensional homeostasis and the malignant phenotype," Cancer Cell **8**(3), 241–254 (2005).
[52]O. Chaudhuri *et al.*, "Extracellular matrix stiffness and composition jointly regulate the induction of malignant phenotypes in mammary epithelium," Nat. Mater. **13**(10), 970–978 (2014).
[53]B. Blanco, H. Gomez, J. Melchor, R. Palma, J. Soler, and G. Rus, "Mechanotransduction in tumour dynamics modeling," Phys. Life Rev. **44**, 279–301 (2023).
[54]A. Gregori *et al.*, "Prognostic significance of integrin subunit alpha 2 (ITGA2) and role of mechanical cues in resistance to gemcitabine in pancreatic ductal adenocarcinoma (PDAC)," Cancers **15**(3), 628 (2023).
[55]J. J. Grzesiak and M. Bouvet, "The $\alpha_2\beta_1$ integrin mediates the malignant phenotype on type I collagen in pancreatic cancer cell lines," Br. J. Cancer **94**(9), 1311–1319 (2006).
[56]I. Jahin, T. Phillips, S. Marcotti, M.-A. Gorey, S. Cox, and M. Parsons, "Extracellular matrix stiffness activates mechanosensitive signals but limits breast cancer cell spheroid proliferation and invasion," Front. Cell Dev. Biol. **11**, 1292775 (2023).
[57]M. J. Ware *et al.*, "Generation of an *in vitro* 3D PDAC stroma rich spheroid model," Biomaterials **108**, 129–142 (2016).
[58]C. R. Drifka, K. W. Eliceiri, S. M. Weber, and W. J. Kao, "A bioengineered heterotypic stroma-cancer microenvironment model to study pancreatic ductal adenocarcinoma," Lab. Chip **13**(19), 3965 (2013).
[59]S.-K. Kim, S. D. Jang, H. Kim, S. Chung, J. K. Park, and H.-J. Kuh, "Phenotypic heterogeneity and plasticity of cancer cell migration in a pancreatic tumour three-dimensional culture model," Cancers **12**(5), 1305 (2020).
[60]J.-H. Lee, S.-K. Kim, I. A. Khawar, S.-Y. Jeong, S. Chung, and H.-J. Kuh, "Microfluidic coculture of pancreatic tumour spheroids with stellate cells as a novel 3D model for investigation of stroma-mediated cell motility and drug resistance," J. Exp. Clin. Cancer Res. **37**(1), 4 (2018).
[61]A. Agrawal *et al.*, "Stromal cells regulate mechanics of tumour spheroid," Mater. Today Bio **23**, 100821 (2023).
[62]L. Chin, Y. Xia, D. E. Discher, and P. A. Janmey, "Mechanotransduction in cancer," Curr. Opin. Chem. Eng. **11**, 77–84 (2016).
[63]M. Ahearne, "Introduction to cell–hydrogel mechanosensing," Interface Focus **4**(2), 20130038 (2014).
[64]C. R. Drifka, A. G. Loeffler, C. R. Esquibel, S. M. Weber, K. W. Eliceiri, and W. J. Kao, "Human pancreatic stellate cells modulate 3D collagen alignment to promote the migration of pancreatic ductal adenocarcinoma cells," Biomed. Microdev. **18**(6), 105 (2016).
[65]A. J. Marzoq, S. A. Mustafa, L. Heidrich, J. D. Hoheisel, and M. S. S. Alhamdani, "Impact of the secretome of activated pancreatic stellate cells on growth and differentiation of pancreatic tumour cells," Sci. Rep. **9**(1), 5303 (2019).
[66]H. J. Hwang, M.-S. Oh, D. W. Lee, and H.-J. Kuh, "Multiplex quantitative analysis of stroma-mediated cancer cell invasion, matrix remodeling, and drug response in a 3D coculture model of pancreatic tumour spheroids and stellate cells," J. Exp. Clin. Cancer Res. **38**(1), 258 (2019).
[67]S.-Y. Jeong, J.-H. Lee, Y. Shin, S. Chung, and H.-J. Kuh, "Coculture of tumour spheroids and fibroblasts in a collagen matrix-incorporated microfluidic chip mimics reciprocal activation in solid tumour microenvironment," PLoS One **11**(7), e0159013 (2016).
[68]S. Lamouille, J. Xu, and R. Derynck, "Molecular mechanisms of epithelial–mesenchymal transition," Nat. Rev. Mol. Cell Biol. **15**(3), 178–196 (2014).
[69]S. Nam, I. A. Khawar, J. K. Park, S. Chang, and H.-J. Kuh, "Cellular context-dependent interaction between cancer and stellate cells in hetero-type multicellular spheroids of pancreatic tumour," Biochem. Biophys. Res. Commun. **515**(1), 183–189 (2019).
[70]P. Cirri and P. Chiarugi, "Cancer associated fibroblasts: The dark side of the coin," Am. J. Cancer Res. **1**(4), 482–497 (2011).
[71]J. Barbazan *et al.*, "Cancer-associated fibroblasts actively compress cancer cells and modulate mechanotransduction," Nat. Commun. **14**(1), 6966 (2023).
[72]J. A. G. Moir, J. Mann, and S. A. White, "The role of pancreatic stellate cells in pancreatic cancer," Surg. Oncol. **24**(3), 232–238 (2015).
[73]M. D. Mohan, N. Latifi, R. Flick, C. A. Simmons, and E. W. K. Young, "Interrogating matrix stiffness and metabolomics in pancreatic ductal carcinoma using an openable microfluidic tumour-on-a-chip," ACS Appl. Mater. Interfaces **16**(16), 20169–20185 (2024).
[74]J. Lu, S. Zhou, M. Siech, H. Habisch, T. Seufferlein, and M. G. Bachem, "Pancreatic stellate cells promote hapto-migration of cancer cells through collagen I-mediated signalling pathway," Br. J. Cancer **110**(2), 409–420 (2014).
[75]Z. Zhang, H. Zhang, X. Liao, and H. Tsai, "*KRAS* mutation: The booster of pancreatic ductal adenocarcinoma transformation and progression," Front. Cell Dev. Biol. **11**, 1147676 (2023).
[76]J. Gore and M. Korc, "Pancreatic cancer stroma: Friend or Foe?," Cancer Cell **25**(6), 711–712 (2014).
[77]B. C. Özdemir *et al.*, "Depletion of carcinoma-associated fibroblasts and fibrosis induces immunosuppression and accelerates pancreas cancer with reduced survival," Cancer Cell **25**(6), 719–734 (2014).
[78]A. D. Rhim *et al.*, "Stromal elements act to restrain, rather than support, pancreatic ductal adenocarcinoma," Cancer Cell **25**(6), 735–747 (2014).
[79]E. Tomás-Bort, M. Kieler, S. Sharma, J. B. Candido, and D. Loessner, "3D approaches to model the tumour microenvironment of pancreatic cancer," Theranostics **10**(11), 5074–5089 (2020).
[80]S. F. Boj *et al.*, "Organoid models of human and mouse ductal pancreatic cancer," Cell **160**(1–2), 324–338 (2015).
[81]A. Papargyriou *et al.*, "Heterogeneity-driven phenotypic plasticity and treatment response in branched-organoid models of pancreatic ductal adenocarcinoma," Nat. Biomed. Eng. (published online) (2024).
[82]K. Kong, M. Guo, Y. Liu, and J. Zheng, "Progress in animal models of pancreatic ductal adenocarcinoma," J. Cancer **11**(6), 1555–1567 (2020).